



Does increased spatial replication above heterogeneous agroforestry improve the representativeness of eddy covariance measurements?

José Ángel Callejas-Rodelas¹, Alexander Knohl^{1,2}, Ivan Mammarella³, Timo Vesala^{3,4}, Olli Peltola⁵, and Christian Markwitz¹

¹University of Göttingen, Bioclimatology, Göttingen, Germany

²Centre for Biodiversity and Land Use, University of Göttingen, Göttingen, Germany

³Institute for Atmosphere and Earth System Research (INAR)/Physics, Faculty of Science, University of Helsinki

⁴Institute for Atmosphere and Earth System Research (INAR)/Forest Science, Faculty of Agriculture and Forestry, University of Helsinki

⁵Natural Resources Institute Finland (LUKE), Latokartanonkaari 9, Helsinki, 00790, Finland

Correspondence: José Ángel Callejas-Rodelas (joseangel.callejasrodelas@uni-goettingen.de)

Abstract. Spatial heterogeneity in terrestrial ecosystems compromises the accuracy of eddy covariance measurements. An example of heterogeneous ecosystems are temperate agroforestry systems, that have been poorly studied by eddy covariance. Agroforestry systems get an increasing attention due to their potential environmental benefits, e.g. a higher carbon sequestration, enhanced microclimate and erosion reduction compared to monocropping agricultural systems. Lower-cost eddy covariance setups might offer an opportunity to reduce this bias by allowing for more spatial replicates of flux towers. The aim of this study was to quantify the spatial variability of carbon dioxide (FC), latent heat (LE) and sensible heat (H) fluxes above a heterogeneous agroforestry system in northern Germany using a distributed network of three lower-cost eddy covariance setups across the agroforestry systems. Fluxes from the three towers in the agroforestry were further compared to fluxes from an adjacent monocropping site. The campaign took place from March 2023 until September 2024. The results indicated that the spatial variability of fluxes was largest for FC , attributed to the effect of different crops (rapeseed, corn and barley) within the flux footprints contributed to the measured fluxes. Differences between fluxes across towers were enhanced after harvest events. However, the temporal variability due to the seasonality and diurnal cycles during the campaign was larger than the spatial variability across the three towers. When comparing fluxes between the agroforestry and the monocropping systems, weekly sums of carbon and evapotranspiration fluxes followed similar seasonality, with peak values during the growing season of $-50 \text{ g C m}^{-2} \text{ week}^{-1}$ and 40 mm week^{-1} , respectively. The variation of the magnitude depended on the phenology of the different crops. The effect size, which is an indicator of the representativeness of the fluxes across the distributed network of three eddy covariance towers against only one, showed in conjunction with the other results that the spatial heterogeneity across the agroforestry was better captured by the network of three stations. This supports previous findings that spatial heterogeneity should be taken into account in eddy covariance studies, and that lower-cost setups may offer the opportunity to bridge this gap and improve the accuracy of eddy covariance measurements above heterogeneous ecosystems.



21

22 1 Introduction

23 The eddy covariance (EC) technique is the central approach to measuring the exchange of energy, trace gases and momentum
 24 between terrestrial ecosystems and the atmosphere (Baldocchi, 2014). The EC technique has been established as a standard
 25 method within the scientific community when rapid-response instruments, capable of measuring wind speed, temperature, and
 26 gas concentrations over the major frequency ranges of the turbulent energy spectrum became commercially available (Rebmann
 27 et al., 2012; Wohlfahrt et al., 2009). These instruments provided the capability to measure the exchange of energy and matter
 28 between the land surface and the atmosphere, driven by eddies of diverse sizes and frequencies (Kaimal and Finnigan, 1994).

29 At a majority of flux sites, a single EC station is installed (Hill et al., 2017) and measurements are made based on the
 30 ergodic hypothesis. The ergodic hypothesis states that covariances (fluxes) calculated over the time domain are equivalent to
 31 covariances calculated over the spatial domain (Higgins et al., 2013). The measured turbulent fluxes and carbon and water
 32 balances, when integrated over a defined time interval, are representative of the tower footprint area corresponding to the
 33 averaging interval (Vesala et al., 2008). This is true for homogeneous sites where the spatial representativeness of fluxes
 34 within the ecosystem of interest is guaranteed with a high degree of confidence (Hurlbert, 1984). However, these conditions of
 35 homogeneity are often not met in many ecologically and socioeconomically interesting sites, such as mixed forests, wetlands,
 36 urban forest interfaces or small-scale farmlands (Finnigan et al., 2003; Hill et al., 2017).

37 Agroforestry (AF) systems are an example of heterogeneous agroecosystems. They combine trees and crops on the same
 38 agricultural land in order to benefit from the presence of trees on the land (Veldkamp et al., 2023; Kay et al., 2019). These
 39 systems offer several benefits, including the potential to prevent wind erosion over crops (van Ramshorst et al., 2022; Böhm
 40 et al., 2014), improve soil fertility (Kanzler et al., 2021), or reduce water loss through evaporation in crops (Kanzler et al., 2019).
 41 Short Rotation Alley Cropping systems, a type of agroforestry, represent an alternative land use practice with the potential to
 42 increase carbon sequestration and improve water use efficiency (WUE) in comparison to conventional monocropping (MC)
 43 agriculture (Markwitz et al., 2020; Veldkamp et al., 2023). These AF systems consist of alternating rows of trees and crops.
 44 The trees employed in these systems are typically fast-growing species, such as poplar (*Populus*) or willow (*Salix*), and are
 45 harvested in cycles of 5-6 years for biomass production. Crops are cultivated in an annual rotation.

46 The spatial configuration of the AF system influences the wind flow regimes within the ecosystem, thereby affecting the
 47 development of turbulence. In many cases, such as over tall vegetation, EC measurements are made within the roughness sub-
 48 layer (RSL), which is, by definition, the atmospheric layer whose dynamics are influenced by the roughness elements and is
 49 located below the inertial sub-layer (Katul et al., 1999). At the AF, the trees act as an effective wind barrier (van Ramshorst
 50 et al., 2022), thus modifying the RSL, creating internal boundary layers (Markwitz, 2021), and changing the characteristics of
 51 turbulence over the field. In addition, the alternation of trees and crops with differing phenologies and canopy heights creates
 52 a heterogeneous distribution of carbon and water vapor sources and sinks. This spatial variability is likely to have an impact



on the measured fluxes, as shown by other authors who have studied the spatial variability of fluxes over different ecosystems, such as pine forest (Katul et al., 1999; Oren et al., 2006) or managed grassland (Peltola et al., 2015).

The location of the EC station within a land use system has been demonstrated to potentially introduce a bias in the measured fluxes (Chen et al., 2011), indicating that a single EC station may not be sufficient to properly account for the spatial variability of fluxes induced by landscape heterogeneity (Katul et al., 1999). The high cost and labor intensity of deploying an EC station are the main reasons for the lack of spatial replicates of EC measurements in many studies (Hill et al., 2017). The infrared gas analyzer (IRGA), the crucial component to measure trace gases, typically accounts for a large proportion of the total installation costs associated with an EC station. Lower-cost EC (LC-EC) setups represent a potential solution to the spatial replication problem of EC measurements, as several EC stations could be deployed for the cost of a single conventional station. LC-EC employ a more economical infrared gas analyser and a sonic anemometer, though these instruments necessitate more rigorous post-processing corrections. Notably, previous studies have demonstrated that LC-EC setup can yield comparable results to those of conventional EC (CON-EC) setups. Hill et al. (2017) compared a custom-built LC-EC setup for CO₂ and H₂O measurements with a CON-EC, with very good agreement in CO₂ and H₂O fluxes. In addition, a different LC-EC setup for H₂O flux measurements was compared with a conventional setup Markwitz and Siebicke (2019), resulting in good agreement in H₂O fluxes. Furthermore, another version of the LC-EC setup deployed in Hill et al. (2017) was extensively validated in the studies of Callejas-Rodelas et al. (2024) and van Ramshorst et al. (2024), with very good agreement in CO₂ fluxes and good agreement in H₂O fluxes.

The LC-EC setups can allow for a higher degree of spatial replication of EC and support conventional EC setups. In addition, they provide a powerful tool for the verification of carbon and water balances in the agricultural and forestry sectors in developing carbon credit markets (Trouwloon et al., 2023). However, the increased uncertainty associated with these setups must be taken into account when calculating balances of energy, carbon, or other variables, and when comparing different land uses. One of the main differences between LC-EC and CON-EC setups is the spectral response of the sensors. The LC-EC setups used in the Callejas-Rodelas et al. (2024), Cunliffe et al. (2022), Hill et al. (2017) and van Ramshorst et al. (2024) studies were characterized by a slower frequency response in CO₂ and H₂O measurements, which induces a higher spectral attenuation in the high-frequency range of the turbulent energy spectrum, compared to CON-EC. The higher attenuation introduces a greater degree of uncertainty when applying spectral corrections, as observed by Ibrom et al. (2007) and Mammarella et al. (2009), among others.

The impact of landscape heterogeneity within a AF system on turbulence, latent heat flux (*LE*), sensible heat flux (*H*) and carbon dioxide flux (*FC*) remains to be examined. Markwitz and Siebicke (2019) and Markwitz et al. (2020) conducted evapotranspiration (*ET*) measurements across multiple AF and MC systems in Northern Germany; however, their measurements were not replicated within a single site. In contrast, in the study of Cunliffe et al. (2022) a total of eight LC-EC setups were deployed in different locations across a landscape of ecological interest (Cunliffe et al., 2022). The objective of this study was to capture the heterogeneity of CO₂ and *ET* fluxes across a semiarid ecosystem, with low magnitude of both CO₂ and *ET* fluxes. To the best of our knowledge, replicated measurements in heterogeneous agroforestry systems are so far lacking.



87 In the present study, a network of three LC-EC setups was deployed, analogous to those utilized in the studies of Callejas-
88 Rodelas et al. (2024), Cunliffe et al. (2022) and van Ramshorst et al. (2024), above an AF site, and one additional LC-EC setup
89 above an adjacent MC site in northern Germany. To the best of our knowledge, this was the first time a distributed network of
90 EC towers has been installed above a temperate agroforestry system. With one and a half years of concomitant flux data from
91 the four EC setups, the objective was to quantify the spatial and temporal variability of *FC* and *LE*, as well as the statistical
92 effect of the increased spatial replication of EC measurements above a heterogeneous site. According to Hill et al. (2017), it
93 is possible to estimate the sampling variability and total uncertainty for an ecosystem with independent spatial replication of
94 EC measurements. This allows for the estimation of the effect size (see Section 2). The present study tested the hypothesis that
95 the increased uncertainty inherent to the use of slower-frequency response sensors in EC measurements can be counteracted
96 by the improvement of spatial replication of EC, which increases its statistical robustness. The objectives of this study were
97 threefold: (i) to quantify the spatial and temporal variability of turbulent fluxes and parameters above AF; (ii) to calculate the
98 effect size of the experimental site, following Hill et al. (2017); and (iii) to compare the ecological functioning of the AF to the
99 MC in terms of carbon and *ET* balances.

100 2 Methods

101 2.1 Site description

102 The measurements were conducted from 1 March 2023 to 19 September 2024 at an agroforestry system located in Wendhausen
103 (Lehre), Lower Saxony, Germany (52.63° N, 10.63° E). Elevation above sea level is 80 m. The field is divided into two distinct
104 systems: an AF system in the north and a MC system in the south (see Fig. 1). The AF system covers an area of 17.3 ha and the
105 MC covers an area of 8.5 ha. The crops cultivated within both systems kept a similar distribution from west to east. In 2023,
106 rapeseed was cultivated at the western side, barley at the eastern side, and corn at the center (Fig. 1a). In 2024, rapeseed was
107 cultivated at the eastern side, barley at the center, and corn at the western side (Fig. 1b). The management of the crops was
108 similar at both AF and MC sites and crops were fertilized. The mean long-term annual precipitation is 617 mm, and the mean
109 annual air temperature is 9.9 °C, for the reference period 1981-2010 at Braunschweig airport ((DWD, 2024)). The soil at both
110 AF and MC sites was classified as a Clay Cambisol, with an organic carbon (SOC) content of 5.8 kg C m⁻² at the MC and
111 and 6.75 kg C m⁻² at the AF. Additionally, the soil bulk density was determined as 1.0 g cm⁻³ at both AF and MC (Veldkamp
112 et al., 2023). Soil characteristic were last measured in 2019.

113 The harvest of rapeseed, barley and corn in the 2023 campaign season occurred on 13 July, 22 August and 26 and Septem-
114 ber. The harvest of rapeseed, barley and corn in the campaign of 2024 took place on 15 July, 5 August and 13 September,
115 respectively. In 2024, rapeseed did not grow well and a mulch cut was carried out, therefore the eastern part of the field was
116 covered by a combination of grasses, bare soil and mulch. Canopy height was estimated from pictures taken during field visits.
117 The maximum height attained by the crops at the peak of their development stage was around 1.5 m for rapeseed, 2.5 m for
118 corn and 1.3 m for barley. The trees present at the AF system are fast-growing poplar (*Populus nigra* × *Populus maximowiczii*)
119 and are typically harvested every 4 to 5 years. The most recent harvest of these trees occurred in 2019. Trees grew from around



120 4.0 m till 5.5 m on average across the measurement period. Further details on the site are provided in Callejas-Rodelas et al.
121 (2024).

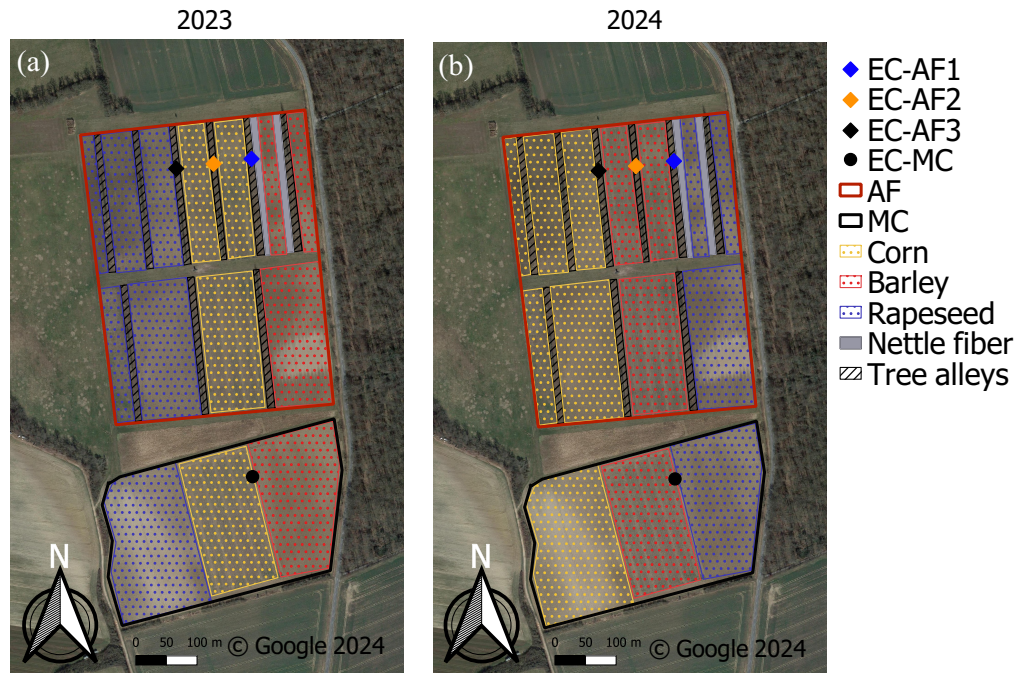


Figure 1. Satellite view and land cover classification of the experimental site for 2023 (a) and 2024 (b), together with the location of the EC stations (blue diamond for EC-AF1, orange diamond for EC-AF2, black diamond for EC-AF3 and black circle for EC-MC). The area bordered red corresponds to the AF system and the area bordered blue to the MC system. Figure created with QGIS v. 3.22, aerial map by Google Satellite Maps. © Google 2024.

122 2.2 Experimental setup

123 Measurements were made at four EC stations, one located at the MC site and three located at the AF site (Fig. 1). The stations
124 are designated as MC, AF1, AF2 and AF3. Each station was equipped with a complete set of meteorological sensors and a
125 LC-EC setup (see Table 1 in Callejas-Rodelas et al., 2024). The measured meteorological variables were air temperature (TA),
126 relative humidity (RH), atmospheric pressure (PA), precipitation (P), global radiation (SW_{IN}), outgoing shortwave (SW_{OUT})
127 and longwave radiation (LW_{OUT}), and net radiation ($NETRAD$). The EC measurement heights were 10 m above ground for
128 AF1, AF2 and AF3, and 3.5 m for MC. Only one photosynthetic active radiation ($PPFD_{IN}$) sensor was installed at AF1,
129 and two barometers for atmospheric pressure measurements were installed at AF1 and AF2. All the stations were equipped
130 with two soil heat flux plates to measure soil heat flux (G) at 5 cm depth. Only one soil heat flux plate was installed at AF3.
131 Radiation sensors were placed in a beam facing south at 9 m height at AF1, AF2 and AF3 and at 3 m height at MC. TA and RH



measurements were taken at 2 m height at all stations. Meteorological data were recorded on CR1000X dataloggers (Campbell Scientific Inc., Logan, UT, USA).

The LC-EC setups consisted of a three-dimensional sonic anemometer for wind measurements (uSonic3-Omni, METEK GmbH, Elmshorn, Germany) and a gas analyzer enclosure. The enclosure consisted of an IRGA for CO₂ mole fraction measurements (GMP343, Vaisala Oyj, Helsinki, Finland), and a RH capacitance cell for RH measurements (HIH-4000, Honeywell International Inc., Charlotte, North Carolina, USA) and was installed at the bottom of the tower. Air was drawn through a 9 m tube at the AF stations and 2.5 m tube at the MC station. Two temperature sensors were installed, one inside the IRGA measuring cell and one inside the enclosure; and two pressure sensors, one to measure differential pressure inside the enclosure and another to measure absolute pressure inside the IRGA measuring cell. Measurements from all components were recorded at 2 Hz frequency on a CR6 datalogger (Campbell Scientific Inc., Logan, UT, USA). A more detailed description of the setup can be found in Callejas-Rodelas et al. (2024).

The GMP343 sensors were calibrated in February 2023 and February 2024. Frequent inspections were performed to clean the tubing, replace filters, measure flow rate, and clean the lens of the GMP343. The nominal flow rate was 5.0 L·min⁻¹ at all AF stations, with some drops due to filter clogging, and 2.2 L·min⁻¹ at the MC before March 14th 2023 and 5.0 L·min⁻¹ thereafter, due to the replacement of the pump by a more powerful one.

During the study period, there were generally large percentages of missing data. Missing data were either short gaps (a few 30-minute periods or a few hours) caused by data filtering during the quality control after flux processing (see Section 2.3.3), or longer gaps (hours to a few days) due to power outages during the winter, mostly at night, at all stations. Due to other technical problems, there were few larger gaps at some stations, in particular a gap of three months from mid-July to early October 2023 at AF3, for *FC* and *LE*.

Although generally recommended in EC studies (Aubinet et al., 2012), no storage terms were considered in the calculation of *FC* and *LE* because no concentration profiles were installed at the stations.

2.3 Flux computation

2.3.1 Pre-processing

Data processing prior to flux calculation included (i) the calculation of CO₂ dry mole fraction measurements from the CO₂ molar density provided by default by the instrument, using some sensor-specific parameters and the observed values of pressure and relative humidity in the measurement system (Callejas-Rodelas et al., 2024); and (ii) the calculation of the H₂O dry mole fraction from relative humidity, temperature and pressure measurements inside the measurement cell using the derivation of Markwitz and Siebicke (2019). More details on the pre-processing steps are given in Callejas-Rodelas et al. (2024) and van Ramshorst et al. (2024).



162 2.3.2 Flux processing

163 H , LE , FC and momentum flux were calculated using the EddyUH software (Mammarella et al., 2016) in its Matlab version
 164 (MATLAB®R2023a, The Mathworks, Inc., Natick, MA, USA). Raw data were de-spiked using limits for absolute differences
 165 between consecutive values. Detrending was performed by block averaging. Wind coordinates were binned into eight sectors
 166 and rotated according to the planar fit correction procedure of Wilczak et al. (2001). Time-lag optimization was performed
 167 through cross-covariance maximization, using predefined windows of 2 to 10 s for CO_2 and 2 to 20 s for H_2O (Callejas-
 168 Rodelas et al., 2024). Low-frequency losses were corrected after Rannik and Vesala (1999) and high-frequency losses after
 169 Mammarella et al. (2009). The latter is based on the determination of the time response of CO_2 and H_2O separately, calculated
 170 from measured co-spectra. In the case of CO_2 the time response determined by the experimental method was similar to the
 171 nominal time response of 1.36 s calculated in Hill et al. (2017) for the GMP343. This time response was used for all flux
 172 calculations for all the three towers. In the case of H_2O the time response was estimated by a exponential fit as a function of
 173 relative humidity. Data quality was flagged from 1 to 9 following Foken et al. (2005).

174 2.3.3 Filtering and gap filling

175 Fluxes were filtered using data with quality flags < 7 to avoid periods with poorly developed turbulence (Foken et al., 2005).
 176 Outliers were removed using a running median absolute deviation (MAD) filter, based on the approach by Mauder et al. (2013),
 177 with a window of two weeks. The q parameter in Eq. (1) of the paper by Mauder et al. (2013) was set as 7.5. The MAD filter
 178 was iterated three times over each time series. Hard upper and lower limits were applied afterwards to remove any additional
 179 outliers not detected by the MAD filter. Values outside the ranges from -100 W m^{-2} to 700 W m^{-2} for H , from -20 W m^{-2}
 180 to 700 W m^{-2} for LE , and from $-55 \mu\text{mol m}^{-2}\text{s}^{-1}$ to $55 \mu\text{mol m}^{-2}\text{s}^{-1}$ for FC , were discarded. Additional hard limits were
 181 applied specifically to winter (November to February) and transition periods (March and October) separately. The aim was to
 182 avoid outliers that went through the previous filters which might bias the application of the gap-filling algorithms. For LE and
 183 H , these limits were of 50 W m^{-2} during winter, and 100 W m^{-2} in March and October. For the FC , these limits were \pm
 184 $10 \mu\text{mol m}^{-2} \text{s}^{-1}$ during winter, and $\pm 15 \mu\text{mol m}^{-2} \text{s}^{-1}$ in March and October. Finally, a friction velocity (U_{STAR} , m s^{-1})
 185 filter was applied to remove periods with non-existent or weak turbulence. The filter of U_{STAR} was applied using REdDyProc
 186 (Wutzler et al., 2018), which removed values based on a U_{STAR} threshold calculated as the maximum of the seasonally derived
 187 U_{STAR} values. These seasonal values were calculated based on Papale et al. (2006). The average U_{STAR} thresholds for the
 188 stations were 0.21, 0.21, 0.18 and 0.16 m s^{-1} for AF1, AF2, AF3 and MC, respectively.

189 The total available data before filtering accounted for 63.4 % (AF1), 80.0 % (AF2), 76.2 % (AF3) and 61.5 % (MC) for
 190 FC and LE , and 85.7 % (AF1), 86.0 % (AF2), 83.1 % (AF3) and 75.9 % (MC) for H , relative to the duration of the whole
 191 measurement campaign. These gaps were due to instrumental or power failure. After filtering, the available data accounted for
 192 36.5 % (AF1), 44.8 % (AF2), 31.3 % (AF3) and 29.2 % (MC), for FC ; 41.6 % (AF1), 50.1 % (AF2), 36.1 % (AF3) and 38.5
 193 % (MC) for LE ; and 61.4 % (AF1), 60.0 % (AF2), 56.4 % (AF3) and 52.3 % (MC) for H . Additional gaps in filtered data were
 194 introduced by rejecting data.



195 Meteorological data were gap-filled at the 30-minute time scale in order to provide complete time series for the variables
196 acting as predictors for the flux gap-filling, with slight differences in the procedure for the different variables of interest. Short
197 gaps of up to one hour were filled using linear interpolation, except for *P*. Missing data at the AF1 station that were available
198 at the MC station, were filled using linear regression models using as predictors the data from the MC, and viceversa. Missing
199 data at AF2 and AF3, but available at AF1, were filled using a similar procedure with AF1 as the reference. Finally, *P*, *TA*,
200 *RH*, vapor pressure deficit (*VPD*), *SW_IN*, wind speed (*WS*) and wind direction (*WD*) were filled at the stations using ERA5-
201 Land re-analysis data (Muñoz-Sabater et al., 2021) as predictors, following the approach implemented in Vuichard and Papale
202 (2015). Linear regression models were derived from the ERA5-Land data and the station data, using the library *pylr2* in Python.
203 The coefficients (slope and intercept) from the linear models were used to calculate the missing values. *PPFD_IN* was filled
204 based on global radiation (*SW_IN*), by multiplying *SW_IN* by the average ratio between *PPFD_IN* and *SW_IN* for the available
205 periods at the site. *P* was filled by multiplying the ERA5-Land data by the ratio between the station data and the re-analysis
206 data, as done in Vuichard and Papale (2015). Possible inaccuracies resulting from this replacement did not contribute to an
207 additional bias in the gap-filled flux time series, as precipitation was not used for gap-filling purposes. A quality flag was
208 developed for meteorological data, with 0 being measured data, 1 being interpolated data, 2 being data filled using the nearby
209 station as a reference, and 2 being data filled with ERA5 as a reference.

210 Gaps in the flux time series were filled using a double-step procedure, analogous to the approach applied in Winck et al.
211 (2023). Short gaps were filled using the Marginal Distribution Sampling method (Reichstein et al., 2005) with the online
212 version of the REddyProc package (Wutzler et al., 2018). Short gaps were considered by taking the filled data with quality
213 flags of 0 (originally measured data) or 1 (highly-reliable filled data). Subsequently, the remaining gaps (flagged with 2 or 3
214 in REddyProc) were filled using a machine learning (ML) tool based on the Extreme-Gradient-Boosting (XGBoost) algorithm
215 (Chen and Guestrin, 2016). The code was adapted from Vekuri et al. (2023) to include *H*, *LE* and *FC*. The predictor variables
216 of the model were the previously filled *TA*, *VPD*, *SW_IN*, *WS* and *WD*. The inclusion of *WD* followed the recommendation
217 of Richardson et al. (2006) to account for the heterogeneity of the site, with different land covers depending on wind sectors
218 potentially contributing to flux variability. A quality flag was developed for flux variables, being 0 measured data, 1 data filled
219 with REddyProc, and 2 data filled with XGBoost. There were two very long gaps, one for AF3 during summer 2023 (mid
220 July until beginning of October) and another for AF1 during winter 2023/24 (beginning of December 2023 until beginning of
221 March 2024), besides gaps of few days duration. Because such long gaps would induce very large uncertainty in any gap-filling
222 method, the analysis considered only measured data and gap-filled data for gaps not exceeding two weeks duration.

223 The error in gap-filled fluxes with XGBoost was taken as the root mean squared error (RMSE) of the modelled data. Table
224 1 shows the RMSE scores for *FC*, *LE* and *H* for all four stations. RMSE was taken as the error attributed to each individual
225 gap-filled 30-minute flux value.



Table 1. Root mean squared error (RMSE) of modeled and measured data, for FC , LE and H , for the four stations used in this study. Note that the error in FC was slightly different across the stations, but the displayed values are similar due to the effect of decimal rounding.

	AF1	AF2	AF3	MC
FC ($\mu\text{mol m}^{-2}\text{s}^{-1}$)	2.8	2.8	2.8	2.8
LE (W m^{-2})	23.2	32.8	19.7	25.7
H (W m^{-2})	14.5	15.2	13.0	14.1

2.3.4 Footprint calculation.

A footprint climatology was calculated for all stations, for five different periods considered in the study: (i) growing season 2023: from March to 13 July 2023, with the latter being the harvest date of rapeseed; (ii) harvest period 2023: from 13 July to 22 September 2023, with the latter being the harvest date of corn; (iii) winter 2023/24: from 22 September 2023 to 1 March 2024; (iv) growing season 2024, from 1 March to 15 July 2024, with the latter being the harvest date of the rapeseed; and (v) harvest period 2024, from 15 July to 19 September 2024. The footprint climatology was calculated using the Python version of the model by Kljun et al. (2015).

The input data to the footprint model comprised non gap-filled wind data (WS , m s^{-1} , and WD , $^\circ$), roughness length (z_0 , m), U_{STAR} , Obukhov length (L , m), the standard deviation of lateral wind speed (V_{SIGMA} , m s^{-1}), boundary layer height (BLH , obtained from ERA5, Hersbach et al. 2023), measurement height (z_m , m), displacement height (d_h , m) and aerodynamic canopy height (h_a , m). Only daytime values were selected based on values of SW_{IN} higher than 10 W m^{-2} . The aerodynamic canopy height was calculated during near-neutral conditions (stability parameter $ZL \leq 0.1$) based on the procedure by Chu et al. (2018). The complete time series of h_a were estimated as described in more detail in van Ramshorst et al. (in prep.). This allowed for a more comprehensive representation of the roughness effects of a varying canopy, therefore it can be considered as a more precise representation compared to the use of a single value representing the average canopy height for the whole site for each time step. d_h and z_0 were estimated as 0.6 and 0.1 times the aerodynamic canopy height, following Chu et al. (2018). The mean values of d_h were 3.1 m at the AF and 0.6 m at the MC, while the mean values of z_0 were 0.5 at the AF and 0.1 m at the MC. A thorough discussion on the uncertainties of the footprint model can be found in Section 4.4.

2.4 Spatial and temporal variability of fluxes and turbulence parameters and effect size

In order to disentangle spatial and temporal variability of fluxes and turbulence parameters across the site, the data were classified in two different ways. Firstly, data were aggregated according to different wind sectors of 30° each, and separated into five time periods as described in the previous paragraph. Secondly, data were grouped in periods of one week, along the whole measurement campaign, without the division into wind sectors. For each of these classifications, coefficients of spatial variation (CVs) were calculated and the variance was partitioned into temporal and spatial components.



250 The CVs were defined as follows

$$251 \quad CV_x = \left[\frac{\overline{< [x(t) - X(t)]^2 >^{\frac{1}{2}}}}{X(t)} \right] \quad (1)$$

252 based on Katul et al. (1999) and Oren et al. (2006). X is the spatial average of variable x across the three towers in the AF
 253 for the respective averaging time interval. Angular brackets ($\langle \rangle$) denote the spatial averaging operator and the overbar denotes
 254 temporal average across all the individual time steps t . This formula was applied to H , LE and FC , and to the standard deviation
 255 of the vertical wind velocity (W_SIGMA , $m\ s^{-1}$), $USTAR$ and WS . The coefficients of variation are dimensionless, normalized
 256 by the spatial average of variable x , such that they can be compared for different variables. Lower limits were set for some of
 257 the variables, in order to avoid biasing the coefficients of variation by some very low fluxes in the denominator of Equation 1.
 258 These limits were $10\ W\ m^{-2}$ for H and LE , $\pm 2\ \mu mol\ m^{-2}\ s^{-1}$ for FC , and $0.5\ m\ s^{-1}$ for U .

259 The partitioning of the variance into temporal and spatial components was done as presented in Peltola et al. (2015) (Eq. 2
 260 therein) based on Sun et al. (2010):

$$261 \quad \sigma_{tot}^2 = \frac{m(n-1)}{m \cdot n - 1} \bar{\sigma}_s^2 + \frac{n(m-1)}{m \cdot n - 1} \sigma_t^2(\xi) = \sigma_s + \sigma_t \quad (2)$$

262 with m the number of temporal data points, n the number of measurement locations, $\bar{\sigma}_s^2$ the time average of the spatial variance,
 263 and $\sigma_t^2(\xi)$ is the temporal variance of the time series of spatial averages ξ . Consequently, the first term on the right hand side of
 264 the equation is equivalent to the spatial variance (σ_s), which includes as well the instrumental variance, while the second term
 265 is equivalent to the temporal variance (σ_t) (Peltola et al., 2015).

266 Furthermore, the effect size (d) was calculated in order to assess the statistical robustness of our distributed network, in
 267 accordance with the hypothesis of Hill et al. (2017) that the enhanced error observed in LC-EC setups can be counteracted by
 268 an improved statistical representativeness of the measurements, provided that the effect size is sufficiently large. In our case,
 269 with the three towers network we calculated d across the three towers inside the AF and between the AF and the MC. d was
 270 calculated, following Hill et al. (2017), as

$$271 \quad d = \frac{f_1 - f_2}{\sigma} \quad (3)$$

272 where f_1 is the flux from ecosystem 1, f_2 is the flux from ecosystem 2 and σ is the pooled standard deviation of data from
 273 both ecosystems. d can be positive or negative. We used daily cumulative sums of gap-filled FC and LE . The value f_1 in Eq.
 274 3 refers to the daily cumulative sums of C ($g\ C\ m^{-2}$) or LE ($W\ m^{-2}$) at the AF, as an average across the three stations, while
 275 f_2 corresponds to the daily cumulative sum of C or LE for AF1 or for MC, depending on the case under study. We calculated
 276 d for two different cases: (i) to test whether fluxes over AF (average across the three towers) were significantly different from
 277 fluxes over MC, in order to compare both ecosystems; and (ii) to test whether fluxes over AF were significantly different from
 278 fluxes from the reference tower AF1, in order to compare the increase in statistical robustness of the distributed network to the
 279 hypothetical case in which only one station was installed at the AF. AF1 was selected as the reference tower because it was the
 280 oldest running tower on site, having been in operation since 2016. σ was calculated as in Hill et al. (2017)

$$281 \quad \sigma = \sqrt{\frac{(n_1 - 1)\sigma_1^2 + (n_2 - 1)\sigma_2^2}{n_1 + n_2 - 2}} \quad (4)$$



where σ_1 and σ_2 are the standard deviations of both datasets being compared, and n_1 and n_2 are the number of data points in each of the datasets. σ was calculated as the error of the daily cumulative sum, from the individual 30-min error in the fluxes (see next section). Afterwards Eq. 4 was applied to get the error for the ensemble of stations being compared.

2.5 Uncertainty of the LC-EC setups

The uncertainty in FC and LE was considered by assigning an error to each 30-min flux value. This error was propagated later on when aggregating data to daily cumulative sums for the effect size calculations. The error was considered differently for measured and gap-filled data. In the case of measured data, the error in the 30-min FC and LE was obtained from the inter-comparison of LC-EC and conventional EC setups in the studies of Callejas-Rodelas et al. (2024) and van Ramshorst et al. (2024). The error was taken as the worst-case slope of the linear regression models between LC-EC and conventional EC setups, separately for FC and LE . It was of 5% for FC and 22% for LE , considered as a relative error for each individual flux value. It is important to note that the error is a systematic deviation from the conventional EC setup, and no random error was considered in these calculations. Therefore, the uncertainty associated with a given flux value is determined by the product of this error value and the magnitude of the flux itself. As an example, a FC of $10 \mu\text{mol m}^{-2} \text{s}^{-1}$ would be expressed as $10 \pm 0.5 \mu\text{mol m}^{-2} \text{s}^{-1}$, and a LE of 100 W m^{-2} would be expressed as $100 \pm 22 \text{ W m}^{-2}$.

In the case of the gap-filled data, the error was addressed differently for the two gap-filling steps. For the data filled with REdDyProc, the error was defined as the standard deviation of the data points used for gap-filling (Wutzler et al., 2018), provided as an output from the REdDyProc processing. In contrast, for the data filled with XGBoost, the individual error in the fluxes was assigned as the RMSE of the modelled data (Table 1). The uncertainty in a cumulative sum was then calculated using error propagation from the single 30-minute uncertainties to the daily sums.

3 Results

3.1 Meteorological conditions

SW_{IN} followed a seasonal cycle, with the maximum magnitude observed at the end of June 2023 (daily means above 300 W m^{-2}), followed by a radiation intensity decrease, reaching the minimum values in winter close to 0 W m^{-2} , and then again increasing until similar maximum values in June 2024 (Fig. 2a). Monthly values of P were large, especially from June to December in 2023, and in July of 2024, with values up to 125 mm (Fig. 2d). There were some very dry months, with P sums lower than 20 mm, especially from March to June in 2024. Compared to the climatological averages (Table 2), all seasons during the measurement period were more rainy than the period 1981-2010, especially during summer and autumn of 2023, when the recorded precipitation was more than three times the reference one (272 mm vs. a reference value of 65 mm for summer 2023, and 218 mm vs. a reference value of 52 mm for autumn 2023). Only spring 2024 was slightly dryer than the climatological reference, with a record of 30 mm of rain instead of 49 mm.



Table 2. Measured and reference climatological averages of *TA* and *P* by seasons. Measured seasonal values were calculated as averages across all four stations at the site. Reference values were taken as the seasonal 1981-2010 climatological average from the German Weather Service (https://opendata.dwd.de/climate_environment/CDC/observations_germany/climate/, last accessed 25-09-2024) from the nearby station at Braunschweig airport (ID 662).

Season	Measured <i>TA</i> (°C)	Measured <i>P</i> (mm)	<i>TA</i> reference (°C)	<i>P</i> reference (mm)
Spring 2023	9.1	102.5	9.1	48.7
Summer 2023	18.7	272.3	17.4	65.0
Autumn 2023	11.9	218.5	9.8	52.0
Winter 2023/24	4.3	198.0	1.7	46.7
Spring 2024	11.8	30.1	9.1	48.7
Summer 2024	18.6	165.8	17.4	65.0

312 *TA* followed a seasonal cycle, with the lowest values in winter (daily means between 0 and 10 °C, with occasional lower
 313 values) and the highest values in July and August of both 2023 and 2024 (daily means around 20 °C). *TA* was slightly larger
 314 at the MC tower than at the other three AF towers during most of the campaign, with enhanced differences in summer and
 315 very small differences in winter. The mean *TA* during the campaign was 12.86 °C at the MC, while it was 12.49 °C at the AF.
 316 The three AF stations showed very similar *TA*. *TA* was higher in all seasons compared to the climatological averages (Table
 317 2), except in spring 2023 in which both values were similar (9.1 °C). Summer 2023 and summer 2024 were slightly warmer
 318 (18.7 and 18.64 °C, respectively) than the reference value (17.4 °C). Autumn 2023, winter 2023/24 and spring 2024 were
 319 clearly warmer than the climatological averages, with 11.9, 4.3 and 11.8 °C vs. the reference values of 9.8, 1.7 and 9.1 °C,
 320 respectively. The absolute difference between measured and historical data was largest in winter.

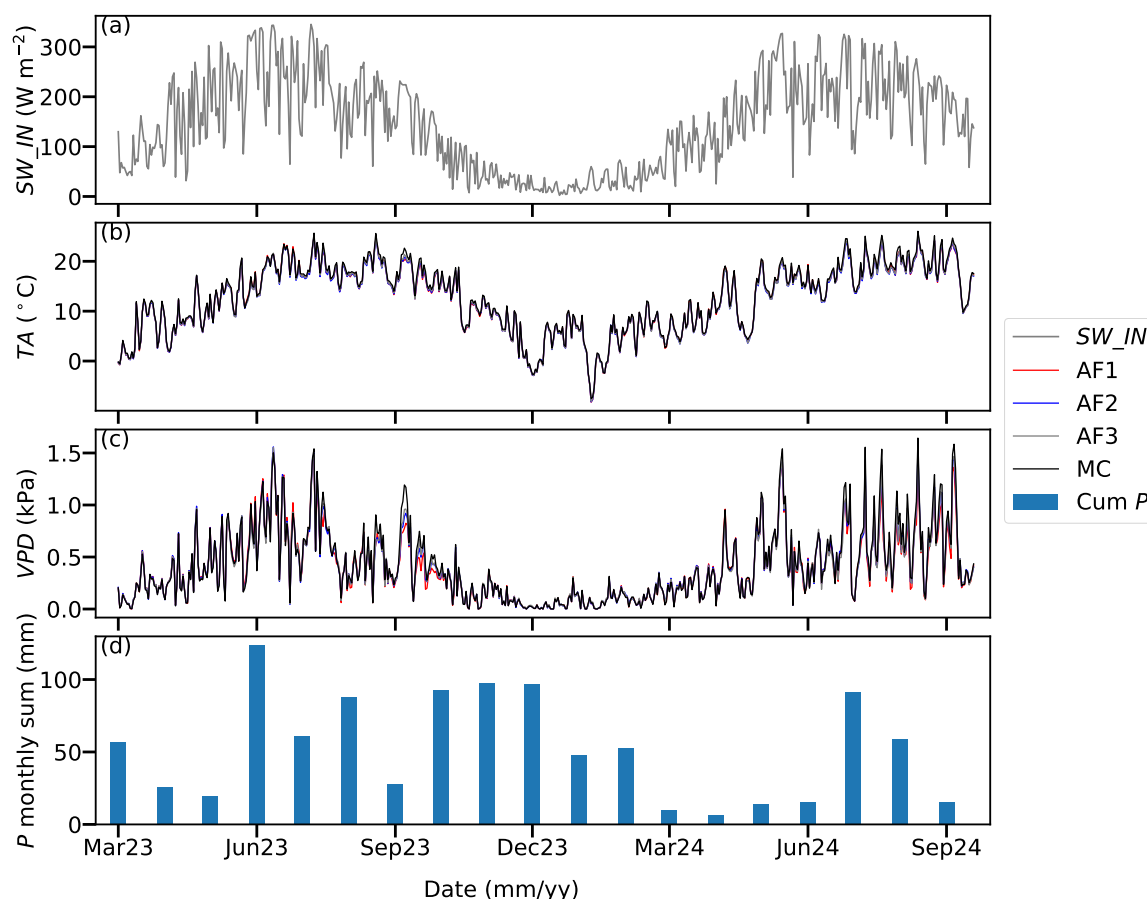


Figure 2. Time series of daily mean meteorological parameter and the cumulative sum of precipitation across the measurement campaign: (a) global radiation (SW_IN), (b) air temperature (VPD), (c) vapor pressure deficit (VPD) and (d) monthly sums of precipitation (P). SW_IN and P were considered as common to all the stations, because the size of the site is small enough to assume homogeneity in these parameters, whereas TA and VPD were plotted separately for all four stations. Data were filtered for outliers using lower and upper limits, gap-filled as detailed in Section 2.3.3, and then aggregated to daily values by taking the daily mean for SW_IN , TA and VPD and the daily sum for P .

321 VPD values also showed a marked seasonality (Fig. 2c). Values were very low in winter, between 0 and 0.2 kPa, and
 322 increased towards summer in both 2023 and 2024, reaching daily means between 1 and 1.5 kPa. VPD was still relatively large
 323 in autumn of 2023, with values of around 0.5 kPa. Comparing the four stations, the MC site experienced a larger VPD from
 324 July to October 2023, while during the rest of the campaign no significant differences were observed across the stations. The
 325 mean VPD was 0.41 kPa at the MC and 0.4 kPa at the AF as an average of the three stations. The differences between the three
 326 AF stations were very small.



3.2 Footprint climatology

The seasonal footprint climatology show the 80 % contributions from the different land uses to the fluxes by all four stations (Fig. 3). All footprints exhibited larger contributions from the western side of the towers in all periods (growing season 2023, harvest period 2023, winter 2023/24, growing season 2024 and harvest period 2024), corresponding to the dominant wind direction at the site. For all periods under consideration, the footprint of the MC tower was smaller than for the three AF towers, due to the lower measurement height. The three stations at the AF exhibited partially overlapping footprints, with different sizes and degrees of similarity depending on the evaluated period. The footprint of the three towers covered approximately four tree rows and four crop rows each. The three towers at the AF presented different footprint sizes, with the largest areas being covered by AF3, followed by AF2 and finally by AF1. The order was the same in all seasons. The footprint from the MC tower covered both the western and eastern fields around the tower, but the contribution was larger from the western part in all seasons. For all stations, there were some contributions to the footprints from the areas beyond the AF or the MC fields. This was especially remarkable in the case of AF3, which had some contributions from the western side of the field in winter 2023/24 (Fig. 3c) and from the northern side of the field in both harvest periods of 2023 and 2024 and the 2024 growing season (Fig. 3b,d,e). However, the contributions of the areas outside the AF were expected to be negligible regarding the interpretation of the results.

The analysis on specific differences between land covers measured by the different stations revealed variations from season to season. In the 2023 growing season, the footprints of AF1, AF2 and AF3 were overlapping the most compared to the other seasons (Fig. 3a). At AF1 predominantly four tree strips, corn, barley and the nettle fiber rows were detected. At AF2, the footprint encompassed a larger area, covering five tree strips, all three crops (rapeseed, corn and barley) plus the nettle fiber was detected. At AF3 the footprint was the most extensive, covering also five tree strips, the three crops and one of the nettle fiber strips, plus some areas beyond the AF site was detected. The overlap of the footprints was more intense between towers AF2 and AF3. The MC tower detected mostly the corn field, with a small contribution of the rapeseed field.

During the harvest period in 2023, the footprint size diminished, partially due to a reduced considered period. The footprint climatology is a weighted average, hence, a longer evaluated period is likely to extend the footprint area. This lead to a reduction in the degree of overlap among the footprints, particularly between AF1 and AF3. AF1 covered three tree strips, corn, barley and nettle fiber; AF2 covered four tree strips, only one row of rapeseed, the whole corn field and a small part of the barley field; AF3 covered also four tree strips, the whole rapeseed field and part of the corn field. The MC tower covered only part of the corn field.

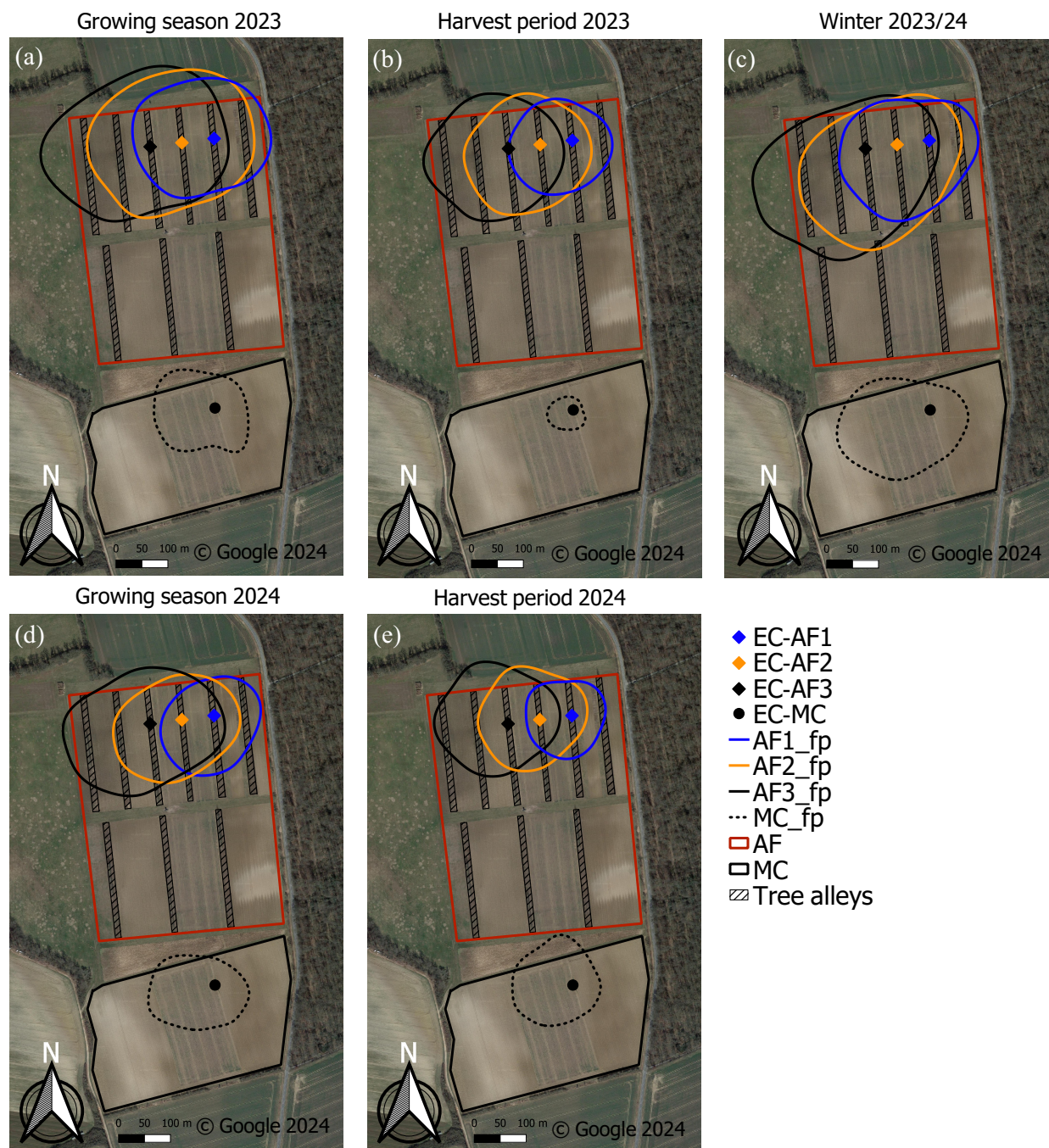


Figure 3. Footprint climatologies, calculated from the model of Kljun et al. (2015), for the three towers at the AF and the tower at the MC (detailed in Section 2.3.4), divided into five different periods: growing season 2023 (a), harvest period 2023 (b), winter period 2023/24 (c), growing season 2024 (d) and harvest period 2024 (e). The lines plotted in the map represent the 80 % contributing areas to the footprint. Figure created with QGIS v. 3.22, aerial map by Google Satellite Maps. © Google 2024.



355 In winter 2023/24 (Fig. 3c), the footprint size increased again for all stations, enhancing the overlap. However, this enhance-
356 ment was not as substantial as the one observed during the 2023 growing season. All crops had been harvested, and only the
357 rapeseed had been sown in the eastern part of the field in September 2023 (Fig. 1b), therefore the remarkable features of this
358 season are that the footprints of both AF1 and AF2 covered one of the rapeseed field rows, together with the nettle fiber, while
359 the footprint of AF3 did not. The other spaces in between tree strips were bare soil during this season. The MC footprint was
360 larger than during the other seasons and covered most of the field in the west of the tower and a small part of the rapeseed field
361 in the east.

362 During the 2024 growing season, the footprints of AF1 and AF2 exhibited an overlap of approximately 50 % of the footprint
363 area, while the overlap between AF1 and AF3 was significantly less (Fig. 3d). AF1 covered rapeseed, nettle fiber, part of the
364 barley field and only three tree strips; AF2 covered part of the corn field and the barley field, plus four tree strips; AF3 covered
365 the whole corn and barley fields and five tree strips. The MC footprint reduced in size compare to the winter period, and was
366 mostly covering the barley field in the west of the station. Finally, during the 2024 harvest period, the footprint size reduced
367 again for all stations, and so did the overlap (Fig. 3e). AF1 covered only part of the barley field and part of the rapeseed field,
368 together with the nettle fiber and two tree strip; AF2 covered most of the barley field and parts of the rapeseed and the corn
369 fields, plus three tree strips; and AF3 covered the corn field, part of the barley field and almost four tree strips. The footprint of
370 the MC was similar to the 2024 growing season (Fig. 3e) covering mostly the barley field and a minor portion of the rapeseed
371 field.

372 3.3 Weekly sums of carbon and evapotranspiration

373 The weekly cumulative sums of *FC* (Fig. 4a) exhibited a marked seasonal behavior and similar variability across the four
374 towers. The seasonal cycle was characterized by the uptake of carbon (negative values) during the growing season and carbon
375 losses (positive values) during winter. The differences were smaller across the three AF towers, with AF1 and AF2 behaving
376 more similar. During the 2023 growing season, there was a strong uptake at all stations of around $-30/-40 \text{ g C m}^{-2}$ per week,
377 from April to September 2023. This was interrupted by the short dry period of three weeks which occurred at the end of May
378 and first half of June of 2023 (DWD, 2024) with the AF site turning to a carbon source (measured by AF2) or to a weak carbon
379 sink (measured by AF1 and AF3). The uptake was stronger at AF3 until mid June, after which MC showed the strongest uptake
380 (-40 to -60 g C m^{-2} per week) for the rest of the growing season. After the harvest of the rapeseed on 13 July 2023, weekly
381 sums reduced in magnitude but were still large at AF1, AF2 and MC (AF3 was missing during this period), and after the harvest
382 of the barley on 22 August 2023 the sums reduced notably. From October 2023 to March 2024, the values were positive and
383 comparable across all stations, indicating a carbon release from the ecosystems. During the 2024 growing season, the carbon
384 uptake was found to be diminished compared to the 2023 growing season. The strongest uptake of around -25 g C m^{-2} per
385 week occurred in July 2024. AF2 and MC showed the strongest uptake during June and July, however, after the harvest of the
386 rapeseed on 15 July, the uptake reduced and AF2 and MC changed their sign towards a carbon source, while AF1 and AF3
387 still showed negative values. After the harvest of the barley on 5 August 2024, the uptake of AF1 and AF3 reduced even more,
388 changing in AF1 towards a carbon source. AF3 kept a CO_2 sequestration behavior until the end of the measurement period.

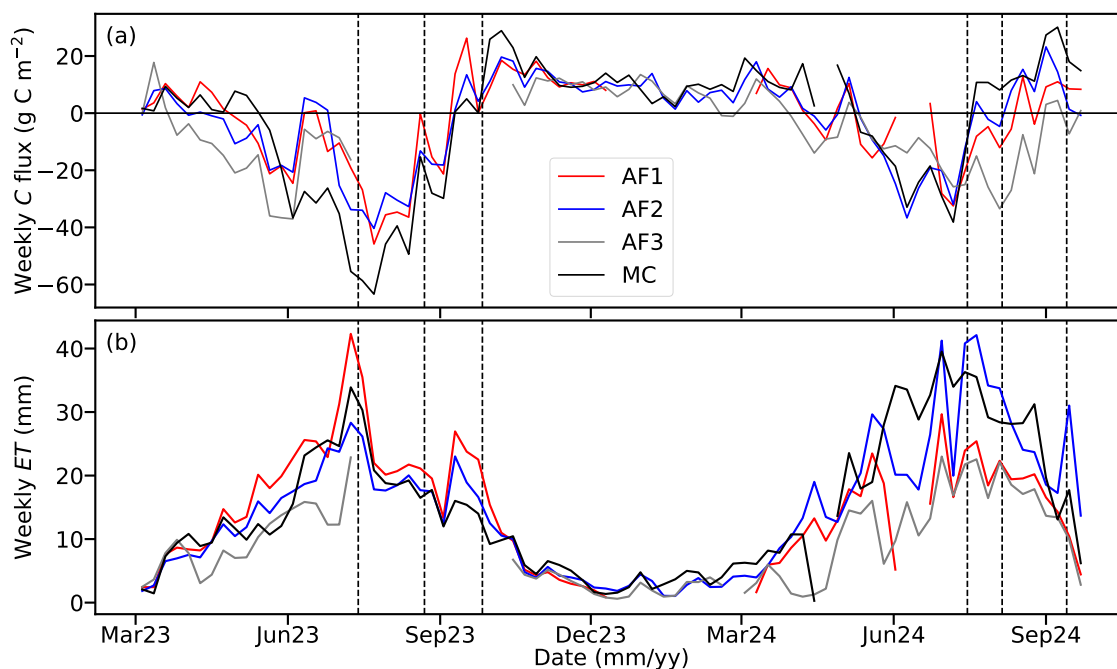


Figure 4. Weekly sums of the net ecosystem carbon exchange as a carbon (C) flux (a) and evapotranspiration (b, *ET*) measured at the four stations, across the measurement campaign. Sums were calculated from the gap-filled time series. Missing values correspond to gaps longer than 2 weeks, which were not considered in the analysis. The horizontal line in sub-plot (a) highlights the zero line, separating the uptake (negative fluxes) from the emission (positive fluxes). Vertical dashed lines represent, from left to right, the harvest dates of rapeseed (13 July 2023), barley (22 August 2023) and corn (26 September 2023) in 2023; and rapeseed (15 July 2024), barley (5 August 2024) and corn (13 September 2024). Due to the requirement of taking only gap-filled data for gaps up to two weeks of duration, there were some missing weeks for all stations and two very long gaps, in summer 2023 for AF3 and in winter 2023/24 for AF1.

389 The weekly cumulative sums of *ET* (Fig. 4b) also exhibited a strong seasonality in all stations and similar variability across
 390 them. During the 2023 growing season, there were increasing *ET* weekly sums from April (values around 10 mm per week)
 391 until the maximum values attained in July, with a magnitude of 30 mm at AF2, AF3 and MC, and 40 mm at AF1. Afterwards
 392 there was a progressive reduction in *ET* especially enhanced after the harvest of the rapeseed on 13 July 2023 and the harvest of
 393 the corn on 26 September 2023. AF1 showed the highest values until October 2023. Thereafter, all stations showed low values
 394 coinciding with the winter period, of around 5 mm per week, until March 2024. During the 2024 growing season, weekly *ET*
 395 was again progressively increasing at all the stations, until they reached the maximum values of 30 and 40 mm. The increase
 396 was only interrupted by a reduction in *ET* in June, more marked at the AF towers. After the peak of the growing season, *ET*
 397 reduced especially after the harvest of the rapeseed on 15 July 2024 and the barley on 5 August 2024. The highest values during
 398 the growing season were found for the MC until July and for AF2 after that, and the reduction in *ET* after the harvest events
 399 was more marked in these two stations. AF1 and AF3 kept lower values and exhibited a more similar behavior.



3.4 Coefficients of variation, spatial and temporal variance

3.4.1 Classification in wind direction bins

The CVs calculated at the half-hourly scale (Eq. 1) were the largest for FC in most of the wind sectors and the evaluated periods, followed by the CVs of LE and H (Fig. 5). The CVs of WS , $USTAR$ and W_SIGMA were low in comparison to the CVs of FC , LE and H . The lowest variability across wind sectors in all periods was found for W_SIGMA , followed by $USTAR$ and WS , with CV values below 0.15 in most of the cases. Within the 2023 growing season, FC showed the largest spatial variability in the eastern and southern wind sectors, with CVs above 0.5 and up to 1.2. LE and H showed similar values of between 0.2 and 0.3, slightly higher for LE (close to 0.4) in the northern wind sectors ($330-60^\circ$). During the 2023 harvest period, no CVs of FC and LE could be calculated due to the absence of data from AF3, therefore only the variability of H and turbulence parameters could be addressed. H showed the largest variability in the northeastern wind sectors ($0-150^\circ$), with values of CVs of above 0.2. In winter 2023/24, the CVs of FC were the largest in the eastern half ($0-180^\circ$), with values between 0.2 and 0.8, while LE and H showed similar values between them; in the sectors $180-270^\circ$ the CVs of LE were the largest, with values up to 0.6, followed by CVs of FC . For the sectors $270-360^\circ$ the CVs of all variables were smaller than 0.3 and very similar across them. During the 2024 growing season, FC showed the largest variability in the eastern ($30-180^\circ$) and northeastern sectors ($330-30^\circ$), with values between 0.4 and 1.7, while the CVs of LE were similar to the CVs of H with a magnitude between 0.2 and 0.4. In the western sector ($180-330^\circ$), however, the CVs of LE were the largest, with values between 0.4 and 0.5, and CVs of FC were similar to the CVs of H . Finally, during the 2024 harvest period, in the eastern sector ($0-180^\circ$) the CVs of FC , LE and H were very similar, with values between 0.2 and 0.4, and in the western sector ($180-360^\circ$) the CVs of LE were slightly larger, between 0.4 and 0.5, and CVs of FC and H remained similar. Both for FC and LE , both variance values were larger during the growing season and the harvest period in both years than during winter, due to the larger magnitude of fluxes. As an overall picture, σ_s was larger than σ_t in the western and northeastern wind sectors. Due to the scope of this analysis, it is important to remark in which wind sectors σ_s was larger than σ_t . Looking first at LE (Fig. 5, mid row) σ_t dominated the variance in all wind sectors during the 2023 growing season. During winter 2023/24, σ_t of LE was larger than σ_s in all sectors except in the bin $210-240^\circ$, when σ_s was much larger than σ_t . During the 2024 growing season, σ_s was larger than σ_t in the wind sectors of $60-90^\circ$ and $300-330^\circ$. Finally, during the harvest period in 2024, the spatial component was larger than the temporal one only in the sector $60-90^\circ$.

Regarding FC (Fig. 5, bottom row), the picture was different compared to LE , with a higher relevance of the spatial component of the variance. During the 2023 growing season σ_t dominated all wind sectors except for the bins $60-90^\circ$ and $150-180^\circ$, but the values of σ_s were close to the values of σ_t in all the eastern sectors. During winter 2023/24, σ_s was larger than σ_t in all wind sectors except $0-30^\circ$, with the largest difference in the eastern ($90-120^\circ$) and southwestern ($210-240^\circ$) sectors, and with relatively large values in the sectors $120-210^\circ$. During the 2024 growing season, σ_s was larger than σ_t in all sectors except in the northwestern ones ($300-360^\circ$), reaching very large values in comparison to other periods (up to $80 \mu\text{mol}^2 \text{m}^{-4} \text{s}^{-2}$) in the eastern half. Finally, during the 2024 harvest period, σ_s was larger than σ_t in the sectors $0-60^\circ$ and $150-240^\circ$, while σ_t dominated in the northwestern sectors.

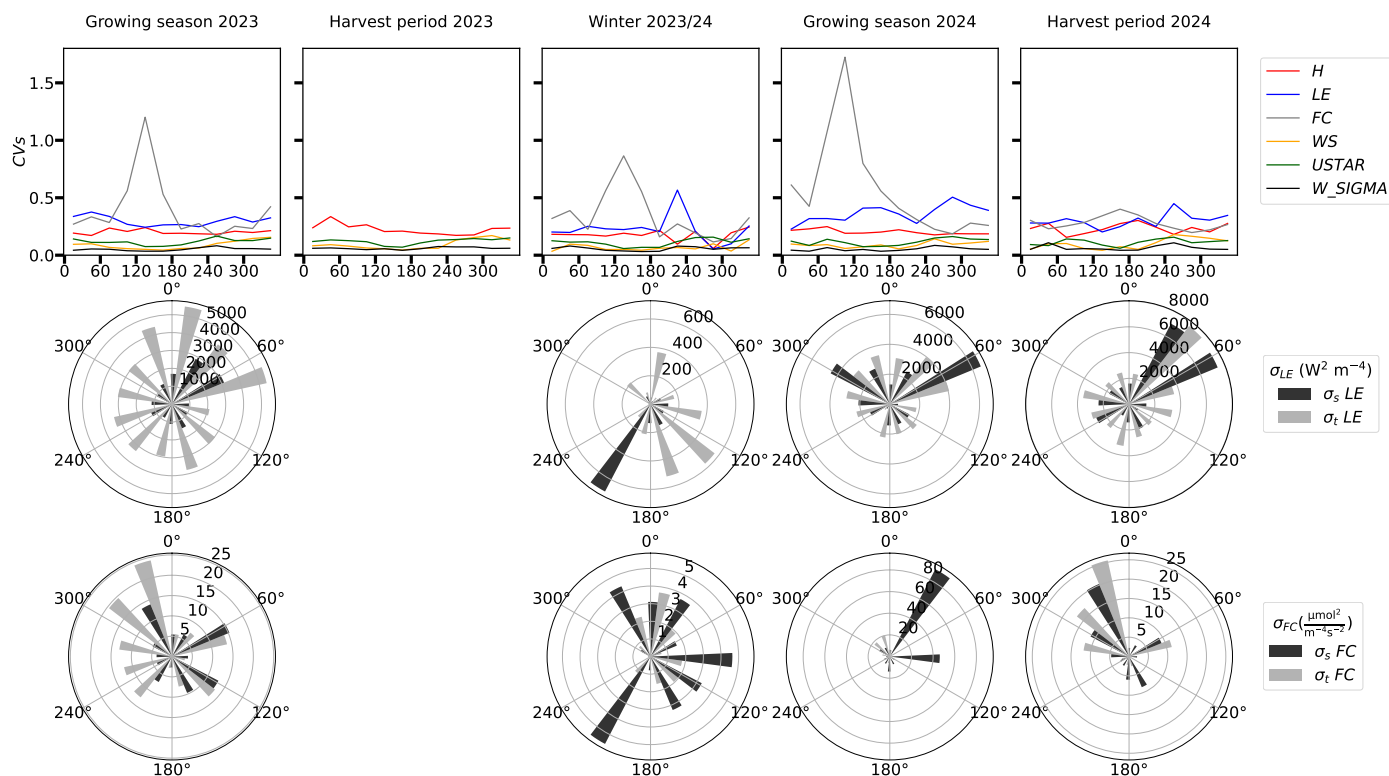


Figure 5. (Top row) Coefficients of variation (CVs), calculated after Oren et al. (2006), for FC , LE and H , WS , $USTAR$, and W_SIGMA ; (mid row) spatial ($\sigma_s LE$) and temporal ($\sigma_t LE$) variance for LE ; (bottom row) spatial ($\sigma_s FC$) and temporal ($\sigma_t FC$) variance for FC . Data were grouped in all cases by wind direction bins of 30° each and separated into the five analysis periods (growing season 2023, harvest period 2023, winter 2023/24, growing season 2024 and harvest period 2024) detailed in Section 2.3.4. Due to the two very long gaps in AF1 and AF3 (see Fig. 4), plus some shorter gaps, there were no data corresponding to the harvest period in 2023 for FC or LE , therefore the sectorial plots for the variance partition are missing. Note that in the first row, due to the large magnitude of some of the CVs of FC , the variability in the lines corresponding to the other variables is more difficult to visualize. Note that the scale is different in the circular plots, depending on the magnitude of what is represented in each season.

3.4.2 Classification in weekly intervals

The weekly CVs across the measurement campaign were largest for FC , with a large difference to the rest of the variables being evaluated (Fig. 6a). The difference was especially remarkable during winter and from March to May 2024. At the beginning of the 2023 growing season, in March and April, the CVs of FC were between 0.3 and 2, much larger than the CVs of LE , while in May, June and until mid July (when the large gap in AF3 started), CVs of FC and LE were similar, with values between 0.2 and 0.5, except for a very large value of 10 the first week of June. In the short evaluated winter period, CVs of FC were very large in comparison to the other variables, with values up to 3.9, and one very large value of 48. However this value could be classified as an outlier because of the larger noise and uncertainty in the winter data. The CVs of LE showed a small variability



and were close to H , with values between 0.1 and 0.3. During the 2024 growing season, in March and April the CVs of FC were large, with values up to 17 in March, while CVs of LE were between 0.3 and 0.5, and CVs of H between 0.2 and 0.3. From May 2024, the CVs of FC were similar to the CVs of LE , with values around 0.5 and slightly lower during the 2024 harvest period, and followed closely by the CVs of H . During the whole campaign, the CVs of $USTAR$, and W_SIGMA were much lower than for H , LE and the FC , similar as shown in Figure 5, with values below 0.2 across the whole period. However, the CVs of \bar{u} were similar to the ones of H during the growing season as well as the 2023 harvest period. After summer 2023 the CVs of \bar{u} reduced their magnitude. The CVs of $USTAR$, and W_SIGMA were the lowest and did not change much during the campaign. In general, there was no clear effect of the harvest event on the variation of CVs for all variables.

With regards to partitioning the variance into its temporal and spatial components, σ_t was higher than σ_s for both LE and FC (Fig. 6b and 6c) during all the evaluated periods. The highest variance was observed during the end of the growing season in both years and during the harvest period in 2024, while the lowest occurred in winter time. During winter, σ_s and σ_t were very similar for both LE and FC . The spatial variance of LE and FC was largest in the summer months of both years. However, the difference between σ_t and σ_s changed from LE to FC . In the case of LE , σ_s was very close to σ_t from March to August 2024, being even higher in some weeks, and decreased largely in the harvest period. In the case of FC , σ_s stayed at very low values in comparison to σ_t during the whole period. The effect of harvest events in 2024 was shown by a lower variance in both temporal and spatial components, especially visible in the case of LE for which σ_s reduced sharply after the harvest of the rapeseed in 2024 (Fig. 6b).

3.5 Effect size and statistical representativeness of the three-towers network

Figure 7 shows the effect size time series, based on the daily sums, for the comparison of FC and LE across the AF and between AF and MC. In the case of the AF evaluation for FC , d_{AF-FC} values were mostly in the range -0.7 to -1.0 in most periods. After May in both years, values started to reduce progressively, reaching -1.3. The values were lowest (more negative) of around -1.4 in July 2024. With respect to the comparison between AF and MC for FC , the dynamics of $d_{AF-MC-FC}$ were similar to the behavior of d_{AF-FC} , with slight differences. The values were always between 0.5 and 1.5, being especially concentrated in the range 0.8-1.0 in the periods of February to May 2023, winter 2023/24, and March, August and September of 2024. In both summers of 2023 and 2024, $d_{AF-MC-FC}$ was larger with values between 1.0 and 1.5. The maximum values were reached in July 2023.

The comparison of LE showed different dynamics (Fig. 7). Regarding the evaluation of d_{AF-LE} , the values were very constant at around -1.0 during 2023 and winter 2023/24. In 2024, a higher variability was observed, but reduced magnitudes (less negative) as compared to d_{AF-FC} . The magnitudes decreased slightly to -0.7 to -0.8 at the end of the campaign, during the months of June, July and September 2024, while August showed again values close to -1.0. With respect to $d_{AF-MC-LE}$, values were in the range 0.7-1.1 most of the time, with a slightly higher variation from March to July 2023. During the 2024 growing season, the variability was lower. In general, $d_{AF-MC-LE}$ varied less than $d_{AF-MC-FC}$ during the whole campaign.

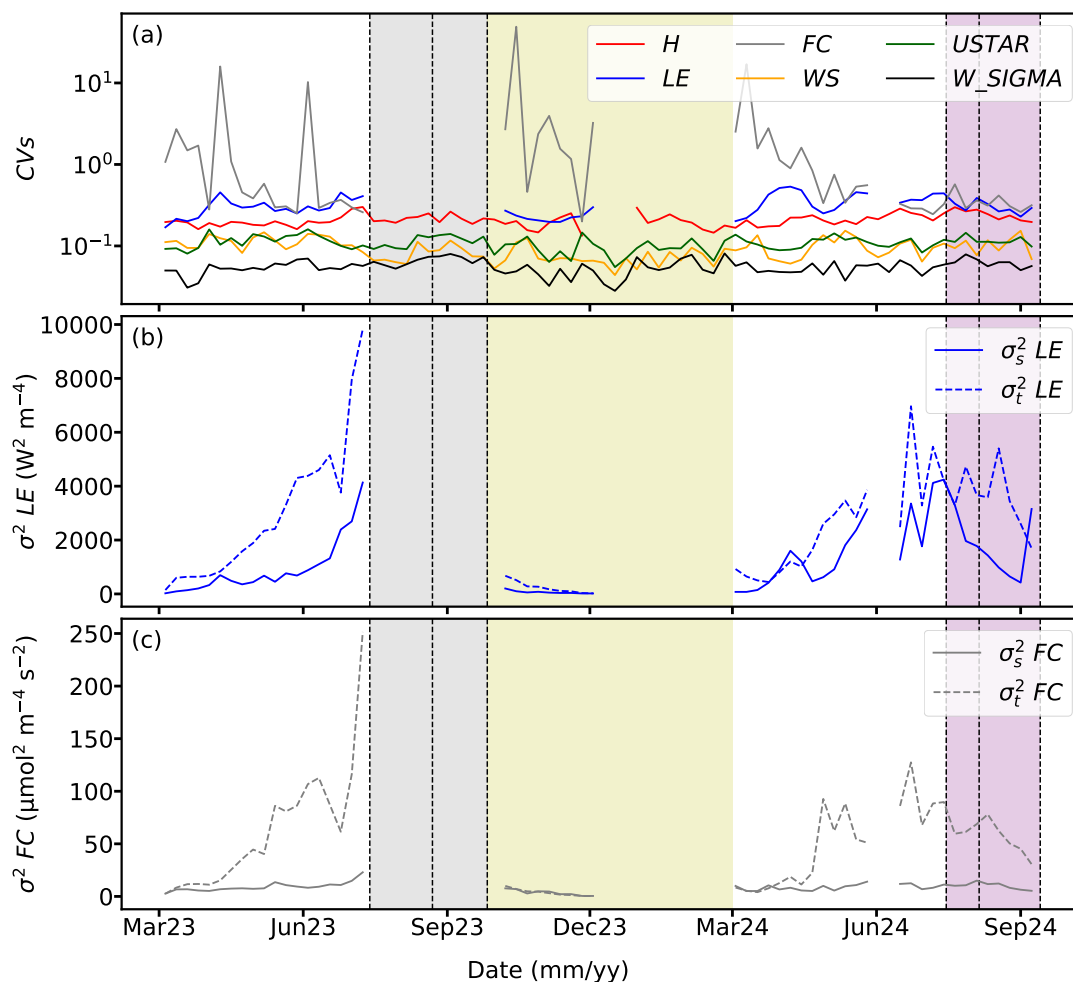


Figure 6. (a) Coefficients of variation (CVs), calculated after Oren et al. (2006), for FC , LE and H , \bar{u} , $USTAR$, and W_SIGMA (logarithmic scale); (b) spatial ($\sigma_s^2 LE$) and temporal ($\sigma_t^2 LE$) variance for LE ; (c) spatial ($\sigma_s^2 FC$) and temporal ($\sigma_t^2 FC$) variance for FC . The plotted values are weekly means calculated at 30-min temporal resolution from the flux time series. Vertical dashed lines represent, from left to right, the harvest dates of the crops in 2023, for rapeseed (13 July 2023), barley (22 August 2023) and corn (26 September 2023); and in 2024, for rapeseed (15 July 2024), barley (5 August 2024) and corn (13 September 2024). Dashed areas correspond to the 2023 harvest period (grey), the winter period (yellow) and the 2024 harvest period (purple), for a better comparison with Figure 5. Due to the two very long gaps in AF1 and AF3 (see Fig. 4), plus some shorter gaps, there were no data corresponding to the harvest period in 2023 for FC or LE and only few weeks of data in the winter period. Note the logarithmic scale in panel (a), introduced due to the large magnitude of some of the CVs of FC for visualization purposes.

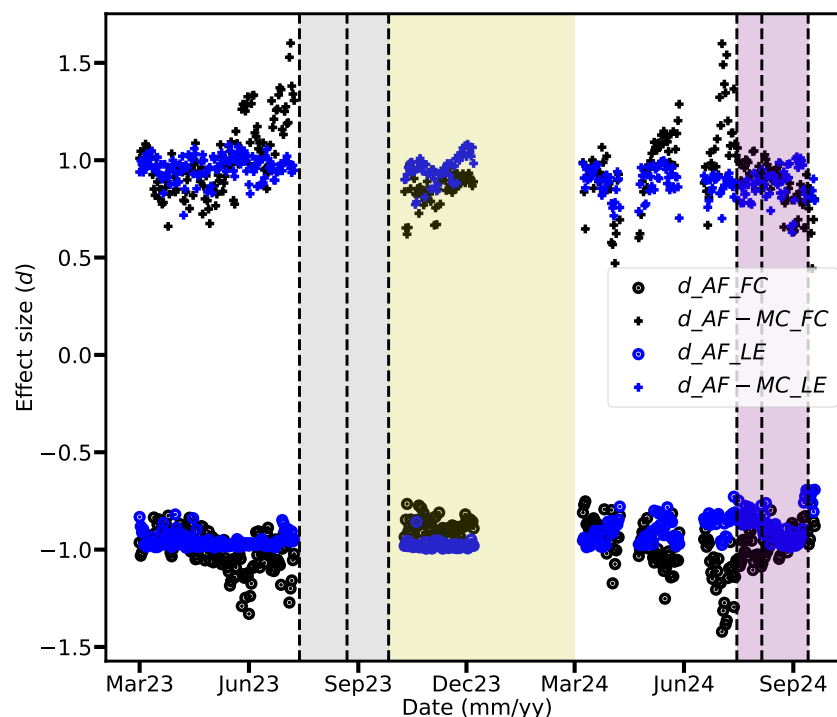


Figure 7. Time series of the effect size (d) for FC and LE . d was calculated according to Eq. 3, based on the daily sums of FC and LE . Black filled circles represent the comparison between AF1 and the average of the three stations at the AF (AF1, AF2 and AF3) for the FC . Black crosses represent the comparison between the average of the three stations at the AF (AF1, AF2 and AF3) and the MC station for FC . Blue filled circles represent the comparison between AF1 and the average of the three stations at the AF (AF1, AF2 and AF3) for LE . Blue crosses represent the comparison between the average of the three stations at the AF (AF1, AF2 and AF3) and the MC station for LE . Vertical dashed lines represent, from left to right, the harvest dates of the crops in 2023, for rapeseed (13 July 2023), barley (22 August 2023) and corn (26 September 2023); and in 2024, for rapeseed (15 July 2024), barley (5 August 2024) and corn (13 September 2024). Dashed areas correspond to the 2023 harvest period (grey), the winter period (yellow) and the 2024 harvest period (purple), as in Figure 6.

474 4 Discussion

475 4.1 Spatial and temporal variability of FC and LE above the AF system

476 Using three distributed EC stations over the same AF system, a small spatial variability in meteorological parameters was
 477 found, but the spatial variability in CO_2 and energy fluxes was larger. The AF site is not very large (19.1 ha) compared to the
 478 median farm size of 29.4 ha in Lower Saxony (Jänicke et al., 2022). The effect of several rows of trees perpendicular to the wind
 479 can significantly influence the microclimatic conditions of different areas in the agricultural field, compared to open croplands
 480 (Kanzler et al., 2019). However, the meteorological conditions measured at the three towers were very similar, probably due
 481 to the fact that all stations were located within the tree strips, and not in between or outside them and due to the small size



of the AF field. The observed variability in *FC* and *LE* should therefore not be attributed to the meteorological drivers, but to the differences in the footprint areas of the three stations. The footprint climatology of the stations partially overlapped (Fig. 3), but the most intense flux contributions originated from an area around the towers. Differences in crop development and management practices could explain most of the spatial variability of the observed fluxes across the three towers throughout the campaign, because of the different crops that were sown in between the tree strips (spatial variability) and the different crop distribution from 2023 to 2024 (temporal variability) (Fig. 1).

The higher spatial variability in turbulent fluxes compared to other turbulence and wind parameters (Fig. 5), especially for *FC* and *LE*, was found also in the studies of Katul et al. (1999) and Oren et al. (2006). This can be explained by the control of stomatal and boundary layer conductances, as well as the more complex nature of sources and sinks for CO₂ and H₂O fluxes (Katul et al., 1999). The larger *CVs* of *FC* at the eastern wind sectors (Fig. 5) during all evaluated periods relate directly to the footprint climatology differences, because the footprints were the most different at the eastern side of the three AF stations (Section 3.2). There was still a relatively large variability in *LE* and *FC*, due to the much smaller size of the footprint climatology area, which led to less overlapping footprints from the three stations (Fig. 5 and 3), therefore higher. The harvest events in 2024 did not seem to affect the *CVs* (Figs. 5 and 6a) compared to the 2024 growing season.

The larger temporal variance, compared to spatial variance, for both *FC* and *LE*, could be explained by the dominance of seasonal and diel patterns of these variables. Spatial variability was important (Sections 3.4.1 and 3.4.2), but it had less relevance than the larger seasonal and diurnal variability. Nonetheless, σ_t was similar to σ_s in winter for both *LE* and *FC*, which can be attributed to the dormant state of the ecosystem, leading to small diel variations and therefore small temporal variations. In summer 2024, for *LE*, σ_s was similar to σ_t , due to the less overlapping areas caused by a reduction in the footprints (Fig. 3) compared to the 2023 growing season, but also to the absence of a fully developed crop in the eastern part of the field, because of the bad growth of rapeseed during this season. This caused weaker *LE* measured especially at tower AF1 and led to a lower spatial variation.

Compared to similar approaches in the literature, Peltola et al. (2015) found a paired temporal and spatial variability in CH₄ fluxes measured at three different heights at a tall EC tower and two additional EC stations over an agricultural landscape. Hollinger et al. (2004) measured fluxes using two towers with non-overlapping footprints in a forest and found that the temporal variability was larger, but the spatial disagreement in *FC* was not negligible, despite the apparent homogeneity of the ecosystem studied. Rannik et al. (2006) also compared *FC* measured from two nearby towers over the same ecosystem, with partially overlapping footprints, and found relevant systematic errors in the daytime fluxes attributed to the variability in the turbulent flow field caused by the complexity of the terrain. These systematic differences were important to attribute long-term uncertainties in the ecosystem C uptake, such as it would happen in the complex AF site of the present study. Davis et al. (2010) investigated heterogeneity in *FC* above an arable land and demonstrated the large imprint of spatial heterogeneity in annual balances of C. Moreover, Soegaard (2003) quantified the annual carbon budget of an agricultural landscape by combining footprint-weighted fluxes and spatial variability in different crops, demonstrating the large potential of spatial heterogeneity to bias annual estimates of fluxes. In the present study, the influence of the different land covers around the towers was detectable, except during the winter period, both for *FC* and *LE*, but the differences were smaller than expected for different crops with



clearly different seasonality. This could be explained by the partially overlapping footprints, as already mentioned, but also to the buffering effect caused by the presence of the trees. Trees were assumed to behave similarly across the AF, so their similar CO₂ and water fluxes attenuated the potentially largest differences in turbulent fluxes that would be expected among the crops without trees.

The weekly cumulative sums of *FC* and *ET* across the campaign (Fig. 4) can be explained by the differences in the phenological state of the crops and the management around the towers. These differences can be directly connected to the previously explained behavior of the *CVs* and partitioning of the variance. Spatially replicated experiments demonstrated the potential to more accurately estimate the uncertainty in turbulent fluxes, such as applied in Hollinger and Richardson (2005). However, the footprint areas of the three stations at the AF in the present study were not homogeneous and they only partially overlap, which means that in practice it is difficult to assess the uncertainty for paired observations as in Hollinger and Richardson (2005). Conversely, the deployment of three towers provided a more comprehensive dataset compared to the single tower approach, and the uncertainty of the AF as a whole could be estimated by calculating the standard deviation of the measured fluxes across the three towers. However, the selection of the exact site of the towers in the present study might not have been optimal (Chen et al., 2011), since footprints were partially overlapping (Fig. 1 and 3). This was due to logistic constraints that precluded the selection of any other location within the AF site, such as in the southernmost part of the field. On the other hand, the purpose of the study was to investigate small scale variability in the highly heterogeneous AF, a goal that was generally accomplished.

Assuming that the trees were growing in a similar way across the whole AF site, the observed variations in weekly sums of carbon and *ET* (Fig. 4) can be attributed to the developmental differences among the crops cultivated around the stations. Specifically, the earlier development of rapeseed in 2023 led to an initial carbon uptake at AF3, because the main footprint covered rapeseed (Fig. 3a). This aligned with the larger *CVs* of *FC* in the eastern side of the field (Fig. 5), and during March and April 2023 (Fig. 6a). However, the earlier growth of rapeseed did not result in increased *ET* in AF3 (Fig. 4b), leading to comparable *CVs* of *LE* for all wind sectors (Fig. 5). This is because rapeseed can maintain a relatively large carbon uptake while using limited water resources (Najibnia et al., 2014). The subsequent development of corn and barley led to similar weekly uptakes of carbon at AF1 and AF2, but a larger *ET* at AF1, leading to a decrease in the *CVs* of *FC* and a modest increase in the *CVs* of *LE*. Besides the partially overlapping footprint (Fig. 3), the reason behind is the different water use efficiency among barley and corn, being lower for barley and therefore explaining similar carbon uptake as corn at a higher *ET* (see e.g. Pohanková et al., 2018). After the short drought in May-June, which affected all three stations by reducing both carbon uptake and *ET* due to water stress, weekly carbon uptakes of AF1 and AF2 and weekly *ET* sums were larger than for AF3 until the harvest period. This can be attributed to corn and barley being less present in the footprint area of AF3 (Fig. 3a). Corn and barley exhibited a more intense physiological activity, immersed in the growing season, while rapeseed was likely at its maturity stage.

The harvest of rapeseed in 2023 had a negligible effect on the carbon uptake of AF1 and AF2 much, but seemed to have an effect on *ET*, which reduced for both stations. This can be attributed to a period of several precipitation events, low *TA* and *VPD* (Fig. 2) which reduced both physiological activity and atmospheric water demand. The harvest of barley and corn reduced the carbon uptake and *ET*. Especially the corn harvest had a large impact because it was the main crop in the footprints of AF1 and



AF2 (Fig. 3b). After the harvest period, the slightly larger difference between the three stations may be an effect of the larger gap-filling uncertainty due to the longer gaps and agrees with an enhanced spatial variance compared to the temporal one (Fig. 6b and c).

In 2024, the very dry spring (Table 2) did not affect weekly sums of *ET* since they were similar to the previous year, but affected weekly sums of *FC*, visible by lower fluxes compared to 2023. In 2024, there was no earlier development of the rapeseed as it occurred in 2023, due to the very wet winter conditions. The variability in *ET* was larger than in 2023 due to less overlapping footprints and due to the difference in rapeseed growth (Fig. 3d). The larger carbon uptake at AF2 as well as larger *ET* (Fig. 4) during all the 2024 growing season was due to the influence of barley and partially corn, while AF1 detected only part of the barley field and the non-well developed rapeseed (Fig. 3c). Carbon uptake and *ET* were smaller at AF3 because corn developed later, but reached similar values as AF1 once corn started to grow. After the harvest of the rapeseed, AF1 and AF2 reduced both their carbon uptake and *ET*, with AF2 turning into a carbon source. The effect was more intense for AF2, explained not by the footprint of AF2 in the rapeseed field (Fig. 3e), but rather by the fact that barley had reached the maturity already and there was a strong ecosystem respiration enhanced due to the rainy and wet conditions, as well as a reduced *ET*. Carbon uptake and *ET* release at AF3, on the other hand, did not detect the effect of the rapeseed harvest, because AF3 was not measuring the corresponding portion of the field (Fig. 3e). AF3 kept a large weekly carbon uptake and similar *ET* due to the presence of the corn in its footprint area (Fig. 3). Afterwards, the harvest of barley reduced the uptake of AF1, turning it onto a carbon source, and of AF3 as well as *ET* due to the footprint covered by both stations (Fig. 3e). *FC* was progressively more positive at all three towers until it reached carbon emissions also for AF1 and AF3 around the harvest of the corn, which was the main crop in the footprint area of AF3.

4.2 Differences in *FC* and *ET* between AF and MC systems

The AF site had typically lower air temperature and higher *RH* than the MC (Fig. 2), because the trees at the AF act as a buffer to keep cooler air temperatures and cooler soil resulting in a larger *RH*. This is pointed out in a review by Quandt et al. (2023). The authors stated that during drought events and under drier and warmer climatic conditions, as projected in future climate scenarios, the buffer effect of the trees in keeping cooler temperatures and more humid air could potentially be enhanced.

C uptake and *ET* release were enhanced at the AF at the beginning of the 2023 growing season, because of the earlier development of the trees and the rapeseed, both present in the footprint of all three AF stations (Fig. 1 and 3a). The MC station was measuring mostly the corn field (Fig. 3a). Corn is a crop with a later development compared to barley or rapeseed (Lokupitiya et al., 2009; Soegaard, 2003), but typically very productive (Hollinger et al., 2005; Lokupitiya et al., 2016). Therefore, carbon uptake was larger at the MC during most of the 2023 growing season after corn started its stronger development phase, later than rapeseed and barley. *ET*, on the other hand, was similar to AF2, indicating a larger water use efficiency. In our study, the short dry period in May/June 2023 occurred when the corn was at its highest development stage. Therefore the corn was not affected as strongly as the rapeseed and barley, which was in a more advanced development stage. In general the whole campaign took place during very wet conditions, which potentially enhanced the ecosystem respiration due to the fostered soil organic matter decomposition, with larger litter amounts at the AF. This, together with a larger respiration from the trees, can



586 explain why AF2, although being surrounded by corn, did not show similar carbon uptake, as the other tower within the AF
 587 system.

588 During the 2023 harvest period, the footprint of the MC station covered only corn, not rapeseed (Fig. 3b). Corn was still
 589 growing during July and August of 2023 at the MC, which explains why at the MC tower very large carbon uptake and *ET*
 590 release was retained, while AF2 and AF1 showed reduced fluxes. In winter carbon and *ET* weekly sums were very similar, due
 591 to the dormant state of the ecosystems as mentioned in the previous section. However, fluxes were very small in magnitude and
 592 it is difficult to attribute clear differences between sites.

593 During the 2024 growing season, carbon uptake at the AF was similar to the MC, which is different to 2023. The magnitude
 594 of the carbon uptake at all stations was lower than in 2023. In 2024, barley was grown in the main footprint area of the MC (Fig.
 595 3d), as well as a portion of the rapeseed field, which did not grow well this year. In general, barley is a crop with less intense
 596 physiological activity than corn (Pohanková et al., 2018), which explains the smaller differences to the AF stations. Also, the
 597 meteorological conditions were very wet in winter with a dry spring. During the harvest period in 2024 the carbon uptake
 598 and *ET* reduced more sharply at the MC than at the AF, after the harvest of the rapeseed, because of its partially contributing
 599 footprint (Fig. 3e). The reduction was more pronounced after the harvest of the barley, which contributed the most to the main
 600 footprint covered by the station.

601 Trees within the AF buffer all the effects of management practices of the crops in between tree strips, since their eco-
 602 physiological activity follows a clear seasonality, similar to forests in comparable climates (Anthoni et al., 2004), and might
 603 partially mask the effect of management in certain portions of the field. Since all three towers at the AF cover similar footprint
 604 areas and the western side of the stations was always predominant in the footprint climatology, only large changes in the
 605 source/sink behavior of the field around them can be detected. During the 2023 growing season the footprint area contributing
 606 to the fluxes (Fig. 3) covered corn, which was harvested at the end of September, so just a small effect on the fluxes was
 607 observed after the harvest of the barley at the end of August (Fig. 4). In 2024, on the other hand, the effect of harvest on a
 608 reduction in carbon and *ET* was more pronounced, because of the earlier development of barley compared to corn.

609 By contrast, in the paper by Callejas-Rodelas et al. (2024), the authors compared 4 months of measurements and both carbon
 610 uptake and *ET* were enhanced at the AF during a measurement campaign from April to August 2022, conducted at the same
 611 site. Similar results were obtained by van Ramshorst et al. (2024), who showed an enhanced carbon uptake and *ET* release at
 612 a grassland AF system compared to a MC grassland. However, they only measured in summer, with enhanced physiological
 613 activity of grasses and trees. The dominant species in the footprint area of the MC stations were rapeseed in Callejas-Rodelas
 614 et al. (2024) and grass in van Ramshorst et al. (2024). These species are known to have a lower physiological activity as
 615 compared to corn (Lokupitiya et al., 2009; Zhang et al., 2014).

616 4.3 Effect size and spatial representativeness of the distributed network

617 The effect size *d* was in most cases between 0.7 and 1.3 (Fig. 7), indicating differences between the evaluated daily sums of *FC*
 618 and *ET* on the order of the pooled standard deviation, therefore leading to a relatively large effect size (Abdaki et al., 2024).
 619 The lower variability of *d* for *LE* than for *FC* across the whole measurement campaign relates directly to the findings discussed



in previous sections, e.g. the FC had the largest spatial variability most of the time. Larger spatial variation in FC influences daily sums which were later on used to calculate d . The increase in spatial variability of FC , which was more pronounced than the change in spatial variability of LE , explained the increase in d during the growing seasons of 2023 and 2024, for both the comparison of AF vs. MC and the comparison of the three stations at the AF.

The larger d values calculated for the comparison between AF and MC than for the comparison between multiple towers at the AF (Fig. 7) can be interpreted as an effect of the larger ecosystem differences between AF and MC than within the AF. The differences within the AF system were a result of the small scale heterogeneity of the AF system. Because differences in means were larger than differences in the standard deviation, d can be interpreted such that a network of three EC towers above the AF allowed a better understanding of the effect of management and smaller scale disturbances inside the AF system. However, at the ecosystem scale comparison, AF vs. MC, the traditional approach with only one EC tower could still be sufficient to detect differences between the two ecosystems.

Low values of d were typically attained during winter months. Then fluxes were small (Fig. 4), which lead to a decrease of both the temporal and spatial variability (Fig. 5 and 6). The small effect of heterogeneity across the sites was likely masked by the larger noise in the data, the longer and more frequent gaps and the larger uncertainty in the gap-filled fluxes (Section 2.3.3).

Several studies addressed spatial representativeness of fluxes and the footprint climatology. These studies focused either in studying RE (Hollinger and Richardson, 2005), in separating ecosystem structure and sampling errors in the spatial variability of fluxes (Oren et al., 2006), in disentangling temporal and spatial variability of fluxes using a single tower approach and footprint modeling (Levy et al., 2020; Soegaard, 2003), in the representativeness of single point measurements at the pixel scale for regional to global scale models (Chasmer et al., 2009; Chen et al., 2009; Wang et al., 2016; Ran et al., 2016), or in studying the effect of diverse meteorological conditions in the footprint climatology and canopy structure (Abdaki et al., 2024). To the best of our knowledge, the study of Cunliffe et al. (2022) was the only one deploying several LC-EC setups, similar to the ones used in our study, and one additional conventional EC setup, to quantify the impact of landscape heterogeneity on turbulent fluxes. They studied a dryland site with very low flux magnitudes, different from our site, and obtained a useful agreement between different LC-EC and the conventional EC setups. The differences between setups were attributed to the heterogeneity of the ecosystem, covered by different bushes and grass species, but a less detailed analysis on spatial and temporal variability of fluxes was performed.

In the EC community, EC replicates are not common (Hill et al., 2017; Stoy et al., 2023). Therefore the effect size of either means or sums of fluxes is typically not estimated. Hill et al. (2017), as the first paper showing the potential of LC-EC setups in increasing spatial replication in EC studies, estimated the effect size through the comparison of the average carbon sequestration and the standard deviation of the cumulative sums, for ideal and non-ideal FLUXNET sites (Baldocchi, 2014). In the present study, the effect size was calculated in a similar way, but based on daily sums and pooled standard deviations (errors) of the 30-min time series. The concept in Hill et al. (2017), therefore, was different, since the measurement errors tend to decrease relative to the aggregation period when cumulative sums are calculated (Moncrieff et al., 1996). Their calculated standard deviation was based on the uncertainty in cumulative sums of half-hourly carbon fluxes and not on time series of higher temporal resolution, e.g. 30 minutes. These time series are commonly characterised by higher variability. Due to this



655 difference in the time scale used in the analysis, their findings on how many towers are needed to properly sample an ecosystem
 656 cannot be compared to ours.

657 In general, there is still an ongoing discussion on how much the landscape heterogeneity affect balances of CO₂ and H₂O
 658 measured by single EC towers. The LC-EC setups could help to bridge the gap of low spatial replication across such hetero-
 659 geneous sites by allowing the installation of multiple setups due to their reduced cost. This could be complementary to other
 660 methodologies developed, to understand the effect of spatial heterogeneity on fluxes measured from single towers, such as in
 661 Levy et al. (2020) or Griebel et al. (2016), or measured with several conventional EC setups (Soegaard, 2003; Hollinger et al.,
 662 2004; Katul et al., 1999; Oren et al., 2006).

663 4.4 Footprint modeling and turbulence dynamics at the AF site

664 The footprint model employed in the present study (Kljun et al., 2015) allowed to understand where the source/sink areas of
 665 CO₂ and H₂O were located, at a basic level. The implementation of the aerodynamic canopy height after Chu et al. (2018)
 666 helped to increase the accuracy of the footprint model to cope with the heterogeneity of the AF site. The three towers at the
 667 AF shared a similar footprint climatology (Fig. 3), if the 80 or 90 % area of the contributions to the footprint were considered.
 668 However, the most intense footprint values, which indicate the largest contribution to the measured fluxes, concentrated in
 669 smaller areas around the towers (Kljun et al., 2002). Therefore, most of the observed variability in the development of *FC* and
 670 *LE* can be attributed to the heterogeneity in the land cover around the stations, with different crops at different phenological
 671 stages during the campaign. The smaller variability of fluxes in winter can be attributed to the absence of crops and the
 672 latency state of the trees. One of the key features of the three towers network is that it allowed to disentangle the effect of
 673 management activities, e.g. crop harvest, therefore providing interesting insights in the smaller scale features caused by the
 674 alternating structure of the AF. The division of data in wind direction bins, as done in e.g. Kutsch et al. (2005), to address the
 675 spatial variability of fluxes, turbulence parameters and both spatial and temporal components of the variance, complemented
 676 the information provided by the footprint maps.

677 Canopy height influences the wind speed and the dynamics of turbulence within the AF (Markwitz, 2021), and therefore
 678 the footprint covered by the towers (Kljun et al., 2015). The footprint area, therefore, is very sensitive to a steep change in the
 679 canopy elements. The increase in tree height from 2023 to 2024 led to a reduction of the footprint size and less overlap between
 680 them (Fig. 3). This, together with differences in crop development and meteorological conditions, contributed to an increase in
 681 the *CVs* of *FC* and *LE*, and showed the relevance of the spatial components of the variance for both flux variables.

682 The parameterization implemented in the model of Kljun et al. (2015) does not allow to consider the effect of spatial hetero-
 683 geneity as represented by roughness length and *U_{STAR}*, which are the basic parameters for an accurate footprint estimation.
 684 This is the main source of uncertainty for the footprint modeling in this study. Due to the structure of the AF, it is likely
 685 that the footprint model overestimates the footprint area, attributing the sources and sinks to areas further beyond what really
 686 contributes to the flux. In addition, footprint estimates are sensitive to the vertical distribution of sources and sinks along the
 687 canopy and to the time air parcels expend within it (Launiainen et al., 2007; Prabha et al., 2008). This is likely happening at
 688 this AF site, due to the structure of the tree rows. A more advanced modeling approach combining, firstly, information on flow



dynamics and spatial structure, with e.g. Large Eddy Simulations, similar as performed in Markwitz (2021) and van Ramshorst et al. (2022), and secondly, footprint modeling by applying the procedure described in Göckede et al. (2006) to account for the spatial heterogeneity in roughness length and friction velocity, would provide more accurate footprint estimates. In addition, if the footprint climatology were aggregated based on weighted footprints, as in Chen et al. (2009), the sources and sinks of carbon and water vapour across the site would be characterized in more detail.

The structure of the AF system influences the flow dynamics and therefore affects the turbulence measurements. An Internal Boundary Layer develops across the field, due to the obstacle represented by the edge of the tree rows (Markwitz, 2021). In the roughness sublayer, tree rows induce persistent waves behind them, thereby enhancing the differences in the turbulence-related parameters WS , $USTAR$, and W_SIGMA . However, the dissimilarities were not larger than for the LE or FC (Fig. 5 and 6), because these were controlled by the very irregular distribution of carbon and water sources/sinks, which had a larger impact than the variability in turbulence statistics. In addition, the canopy structure and the spatial heterogeneity at the AF could potentially lead to a large storage of carbon and energy. The storage terms were not accounted for, although they might be relevant at the edges between crops and trees and within the tree rows, which are very dense and therefore less coupled with the atmosphere. All of it might influence advection in horizontal and vertical directions (Mammarella et al., 2007; Aubinet et al., 2010; Feigenwinter et al., 2008), however, it was not possible to account for those terms with the current datasets.

Furthermore, the sensor location bias, defined as the uncertainty caused by measuring only at one point above a heterogeneous site, also depends on the stability conditions (Chen et al., 2011). Under more unstable conditions, the footprint size would decrease and the location bias of each of the towers would increase, better justifying the use of several EC towers to better sample the whole ecosystem. A more detailed study on stability regimes, footprint size and spatial variability of fluxes would inform on this feature, but it was not performed in this study due to the limited data availability and the difficulty in gap-filling turbulence parameters needed to classify stability regimes, such as Obukhov length. With longer time series and more complete turbulence and footprint information, some of the previously detailed shortness of this study could be addressed.

4.4.1 Errors in FC , LE and H

The errors that affect the flux calculation are difficult to disentangle as they propagate through the whole processing routine, from the raw data measurements until the final flux corrections. Therefore, the uncertainty in the use of LC-EC was assigned, for the measured fluxes, based on the previous inter-comparison studies of Callejas-Rodelas et al. (2024) and van Ramshorst et al. (2024), as detailed in Section 2.5. This procedure is similar to the approach applied in Peltola et al. (2015), where they used a previous instrument cross-comparison campaign (Peltola et al., 2014) to assign instrumental uncertainty to the setups they deployed. However, the uncertainty in the use of LC-EC, defined in relation to conventional EC, was obtained during a specific campaign and under specific site conditions, hence there might be a bias in the LC-EC error attribution. Additionally, the uncertainty in the gap-filled fluxes was calculated as explained in Section 2.5, by assigning individual errors to the 30-min fluxes, which can then be propagated when performing the daily cumulative sums. This was detailed as a first attempt on how to easily evaluate errors and propagate them through cumulative sums whenever a new EC setup has been compared to conventional EC setups and balances of carbon or ET are calculated using gap-filled data.



Focusing on the uncertainty in the gap-filling procedure, the presence of very long gaps, especially affecting tower 3 at the AF, would have had largely increased the uncertainty in the data (Lucas-Moffat et al., 2022) if all the time series were filled. Therefore, only measured data and gaps shorter than two weeks were used, which did not allow for a complete spatial heterogeneity study, mainly because of the missing data for AF3 during the harvest period 2023. Using the combination of both REddyProc for very short gaps and the XGBoost model for long gaps was the optimal solution found for this study, similar as done in Winck et al. (2023), and it allowed to assign individual errors to each 30-min flux, as explained in Section 2.5. Additionally, using more strict filtering criteria, such as a higher *USTAR*-threshold or a lower quality flag, would on the one hand provide data of better quality, but would on the other hand increase the uncertainty due to gap-filling of a higher number of gaps.

We used *TA*, *SW_IN* and *VPD* as predictors for gap-filling, which are generally recognized as the main drivers of CO_2 and H_2O fluxes (Vekuri et al., 2023; Wutzler et al., 2018). *WS* was used because of its influence on the development of turbulence and on the spatial information carried by eddies, especially above a very rough surface such as the AF and wind direction was selected to account for the spatial heterogeneity across the different measurement locations of the towers (Richardson et al., 2006). Other meteorological variables were either less relevant for the analysis, such as atmospheric pressure, or more complex to gap-fill, such as net radiation.

Random error (RE) was not considered directly in this analysis, however, it was partially accounted for indirectly when calculating standard deviations of the time series. In addition, RE decreases with increasing length of the datasets (Moncrieff et al., 1996), therefore it becomes less relevant for longer term assessment of carbon and *ET* balances. Also, the approach implemented in e.g. Richardson et al. (2006) and Hollinger and Richardson (2005) treated RE either with similar conditions in consecutive days, or with the approach of two independent towers, but in the present study the towers had partially overlapping footprints and different land covers around them, hence, cannot be considered as independent.

5 Conclusions

This study shows for the first time 1.5 years of measurements from a distributed network of three EC towers above a temperate heterogeneous agroforestry system and a comparison to an adjacent monocropping agricultural system. The use of three EC stations allowed to capture the spatial and temporal variability across the site, which especially affected *FC*. The main differences were attributed to the different developmental stages of the crops across seasons, with larger disturbances of *FC* and *LE* after harvest events. Because of the high degree of spatial heterogeneity, it was important to have a broader footprint coverage to capture small scale differences at the AF. Furthermore, binning the data in wind direction sectors and weeks allowed us to have a detailed picture on the temporal and spatial components of the variance and the coefficients of spatial variation, given that the differences between the different stations were small enough to be masked if a less resolved analysis had been performed.

Secondly, this study included a complex gap-filling procedure which complemented previously published recommendations on how to work with lower-cost EC data. The datasets gathered during the campaign and the processing scheme added value



756 to the data collection of the project, from previous years of measurements, above several agroforestry and monocropping sites.
757 Future research will address in more detail the contrast between different agroforestry and monocropping sites, with more
758 years of data and under a broader range of meteorological conditions.

759 Finally, the footprint coverage required to capture the spatial heterogeneity across the AF, and within the AF and MC, was
760 improved thanks to the use of lower-cost EC setups. We proved satisfactorily the hypothesis that the degree of uncertainty
761 introduced by the use of slower-response gas analyzers for CO₂ and H₂O was counteracted by the better representation of all
762 processes occurring within the AF system. Therefore, we recommend the installation of multiple EC setups, including lower-
763 cost setups, anytime when the degree of heterogeneity of an ecosystem is large. An added value in future studies would be to
764 compare overlapping and non-overlapping measurements in terms of footprint.

765 *Code and data availability.* Data corresponding to this publication, as well as the codes to analyze results and prepare the figures for this
766 publication are available at Zenodo, <https://doi.org/10.5281/zenodo.14855288> (Callejas-Rodelas et al., 2025).

767 *Author contributions.* JACR performed the measurements, data analysis and manuscript writing. AK and CM wrote the project proposal,
768 contributed to data analysis and manuscript editing. IM, TV and OP contributed to data analysis and manuscript editing.

769 *Competing interests.* The authors declare that they have no known competing financial interests or personal relationships that could have
770 appeared to influence the work reported in this paper.

771

772 *Acknowledgements.* We wish to acknowledge the funding agencies for providing the necessary funds to run out this research, as well as the
773 technical support in the field work received by Marek Peksa, Frank Tiedemann, Edgar Tunsch, Dietmar Fellert, and student assistants (Bio-
774 climatology group) from the University of Göttingen. We wish to acknowledge as well the support from the team of the Micrometeorology
775 Group at the University of Helsinki and from LUKE in Helsinki.

776 *Financial support.* This research was supported by the German Federal Ministry of Education and Research (BMBF, project BonaRes,
777 Module A, SIGNAL 031B1063A). This project also received funding from the European Unions' Horizon 2020 research and innovation
778 program under Grant Agreement No. 862695 EJP SOIL, the German Academic Exchange Service (DAAD), and the Reinhard-Süring-

<https://doi.org/10.5194/egusphere-2025-810>

Preprint. Discussion started: 11 March 2025

© Author(s) 2025. CC BY 4.0 License.



779 Foundation (RSS), affiliated to the German Weather Society and ICOS-Finland by University of Helsinki. Olli Peltola acknowledges Research
780 Council of Finland for funding (grant no. 354298).



781 References

- 782 Abdaki, M., Sanchez-Azofeifa, A., Vargas, R., Ludwig, R., and Hamann, H. F.: Spatial and temporal variation of three Eddy-Covariance flux
 783 footprints in a Tropical Dry Forest, *Agricultural and Forest Meteorology*, 345, 109–863, <https://doi.org/10.1016/j.agrformet.2023.109863>,
 784 2024.
- 785 Anthoni, P. M., Knohl, A., Rebmann, C., Freibauer, A., Mund, M., Ziegler, W., Kolle, O., and Schulze, E.: Forest and agricultural
 786 land-use-dependent CO₂ exchange in Thuringia, Germany, *Global Change Biology*, 10, 2005–2019, [https://doi.org/10.1111/j.1365-](https://doi.org/10.1111/j.1365-2486.2004.00863.x)
 787 2486.2004.00863.x, 2004.
- 788 Aubinet, M., Feigenwinter, C., Heinesch, B., Bernhofer, C., Canepa, E., Lindroth, A., Montagnani, L., Rebmann, C., Sedlak, P., and
 789 Van Gorsel, E.: Direct advection measurements do not help to solve the night-time CO₂ closure problem: Evidence from three differ-
 790 ent forests, *Agricultural and Forest Meteorology*, 150, 655–664, <https://doi.org/10.1016/j.agrformet.2010.01.016>, 2010.
- 791 Aubinet, M., Feigenwinter, C., Heinesch, B., Laffineur, Q., Papale, D., Reichstein, M., Rinne, J., and Van Gorsel, E.: Nighttime Flux Cor-
 792 rection, in: *Eddy Covariance: A Practical Guide to Measurement and Data Analysis*, edited by Aubinet, M., Vesala, T., and Papale, D.,
 793 Springer Netherlands, Dordrecht, <https://doi.org/10.1007/978-94-007-2351-1>, 2012.
- 794 Baldocchi, D.: Measuring fluxes of trace gases and energy between ecosystems and the atmosphere - the state and future of the eddy
 795 covariance method, *Global Change Biology*, 20, 3600–3609, <https://doi.org/10.1111/gcb.12649>, 2014.
- 796 Böhm, C., Kanzler, M., and Freese, D.: Wind speed reductions as influenced by woody hedgerows grown for biomass in short rotation alley
 797 cropping systems in Germany, *Agroforestry Systems*, 88, 579–591, <https://doi.org/10.1007/s10457-014-9700-y>, 2014.
- 798 Callejas-Rodelas, J. Á., Knohl, A., van Ramshorst, J., Mammarella, I., and Markwitz, C.: Comparison between lower-cost and conventional
 799 eddy covariance setups for CO₂ and evapotranspiration measurements above monocropping and agroforestry systems, *Agricultural and*
 800 *Forest Meteorology*, 354, 110–86, <https://doi.org/10.1016/j.agrformet.2024.110086>, 2024.
- 801 Callejas-Rodelas, J. Á., Knohl, A., Mammarella, I., Vesala, T., Peltola, O., and Markwitz, C.: Dataset of the journal article "Does
 802 increased spatial replication above heterogeneous agroforestry improve the representativeness of eddy covariance measurements?",
 803 <https://doi.org/10.5281/ZENODO.14855287>, 2025.
- 804 Chasmer, L., Barr, A., Hopkinson, C., McCaughey, H., Treitz, P., Black, A., and Shashkov, A.: Scaling and assessment of GPP from MODIS
 805 using a combination of airborne lidar and eddy covariance measurements over jack pine forests, *Remote Sensing of Environment*, 113,
 806 82–93, <https://doi.org/10.1016/j.rse.2008.08.009>, 2009.
- 807 Chen, B., Black, T. A., Coops, N. C., Hilker, T., (Tony) Trofymow, J. A., and Morgenstern, K.: Assessing Tower Flux Footprint Cli-
 808 matology and Scaling Between Remotely Sensed and Eddy Covariance Measurements, *Boundary-Layer Meteorology*, 130, 137–167,
 809 <https://doi.org/10.1007/s10546-008-9339-1>, 2009.
- 810 Chen, B., Coops, N. C., Fu, D., Margolis, H. A., Amiro, B. D., Barr, A. G., Black, T. A., Arain, M. A., Bourque, C. P.-A., Flanagan,
 811 L. B., Lafleur, P. M., McCaughey, J. H., and Wofsy, S. C.: Assessing eddy-covariance flux tower location bias across the Fluxnet-
 812 Canada Research Network based on remote sensing and footprint modelling, *Agricultural and Forest Meteorology*, 151, 87–100,
 813 <https://doi.org/10.1016/j.agrformet.2010.09.005>, 2011.
- 814 Chen, T. and Guestrin, C.: XGBoost: A Scalable Tree Boosting System, in: *Proceedings of the 22nd ACM SIGKDD International Conference*
 815 *on Knowledge Discovery and Data Mining*, pp. 785–794, ACM, San Francisco California USA, <https://doi.org/10.1145/2939672.2939785>,
 816 2016.



- 817 Chu, H., Baldocchi, D. D., Poindexter, C., Abraha, M., Desai, A. R., Bohrer, G., Arain, M. A., Griffis, T., Blanken, P. D., O'Halloran, T. L.,
818 Thomas, R. Q., Zhang, Q., Burns, S. P., Frank, J. M., Christian, D., Brown, S., Black, T. A., Gough, C. M., Law, B. E., Lee, X., Chen,
819 J., Reed, D. E., Massman, W. J., Clark, K., Hatfield, J., Prueger, J., Bracho, R., Baker, J. M., and Martin, T. A.: Temporal Dynamics of
820 Aerodynamic Canopy Height Derived From Eddy Covariance Momentum Flux Data Across North American Flux Networks, *Geophysical*
821 *Research Letters*, 45, 9275–9287, <https://doi.org/10.1029/2018GL079306>, 2018.
- 822 Cunliffe, A. M., Boschetti, F., Clement, R., Sitch, S., Anderson, K., Duman, T., Zhu, S., Schlumpf, M., Litvak, M. E., Brazier, R. E.,
823 and Hill, T. C.: Strong Correspondence in Evapotranspiration and Carbon Dioxide Fluxes Between Different Eddy Covariance Sys-
824 tems Enables Quantification of Landscape Heterogeneity in Dryland Fluxes, *Journal of Geophysical Research: Biogeosciences*, 127,
825 <https://doi.org/10.1029/2021JG006240>, 2022.
- 826 Davis, P., Brown, J. C., Saunders, M., Lanigan, G., Wright, E., Fortune, T., Burke, J., Connolly, J., Jones, M., and Osborne, B.: Assessing the
827 effects of agricultural management practices on carbon fluxes: Spatial variation and the need for replicated estimates of Net Ecosystem
828 Exchange, *Agricultural and Forest Meteorology*, 150, 564–574, <https://doi.org/10.1016/j.agrformet.2010.01.021>, 2010.
- 829 DWD: Deutscher Wetterdienst climatological means, [https://opendata.dwd.de/climate_environment/CDC/observations_germany/climate/
830 multi_annual/mean_81-10/](https://opendata.dwd.de/climate_environment/CDC/observations_germany/climate/multi_annual/mean_81-10/), 2024.
- 831 Feigenwinter, C., Bernhofer, C., Eichelmann, U., Heinesch, B., Hertel, M., Janous, D., Kolle, O., Lagergren, F., Lindroth, A., Minerbi,
832 S., Moderow, U., Mölder, M., Montagnani, L., Queck, R., Rebmann, C., Vestin, P., Yernaux, M., Zeri, M., Ziegler, W., and Aubinet,
833 M.: Comparison of horizontal and vertical advective CO₂ fluxes at three forest sites, *Agricultural and Forest Meteorology*, 148, 12–24,
834 <https://doi.org/10.1016/j.agrformet.2007.08.013>, 2008.
- 835 Finnigan, J. J., Clement, R., Malhi, Y., Leuning, R., and Cleugh, H.: A Re-Evaluation of Long-Term Flux Measurement Techniques Part I:
836 Averaging and Coordinate Rotation, *Boundary-Layer Meteorology*, 107, 1–48, <https://doi.org/10.1023/A:1021554900225>, 2003.
- 837 Foken, T., Göckede, M., Mauder, M., Mahrt, L., Amiro, B., and Munger, W.: Post-Field Data Quality Control, in: *Handbook of Mi-*
838 *crometeorology*, edited by Lee, X., Massman, W., and Law, B., vol. 29, pp. 181–208, Kluwer Academic Publishers, Dordrecht,
839 https://doi.org/10.1007/1-4020-2265-4_9, series Title: *Atmospheric and Oceanographic Sciences Library*, 2005.
- 840 Griebel, A., Bennett, L. T., Metzen, D., Cleverly, J., Burba, G., and Arndt, S. K.: Effects of inhomogeneities within the flux footprint on
841 the interpretation of seasonal, annual, and interannual ecosystem carbon exchange, *Agricultural and Forest Meteorology*, 221, 50–60,
842 <https://doi.org/10.1016/j.agrformet.2016.02.002>, 2016.
- 843 Göckede, M., Markkanen, T., Hasager, C. B., and Foken, T.: Update of a Footprint-Based Approach for the Characterisation of Complex
844 Measurement Sites, *Boundary-Layer Meteorology*, 118, 635–655, <https://doi.org/10.1007/s10546-005-6435-3>, 2006.
- 845 Hersbach, H., Bell, B., Berrisford, P., Biavati, G., Horányi, A., Muñoz Sabater, J., Nicolas, J., Peubey, C., Radu, R., Rozum, I., Schepers, D.,
846 Simmons, A., Soci, C., Dee, D., and Thépaut, J.-N.: ERA5 hourly data on single levels from 1959 to present. Copernicus Climate Change
847 Service (C3S) Climate Data Store (CDS)., 10.24381/cds.adbb2d47, 2023.
- 848 Higgins, C. W., Katul, G. G., Froidevaux, M., Simeonov, V., and Parlange, M. B.: Are atmospheric surface layer flows ergodic?, *Geophysical*
849 *Research Letters*, 40, 3342–3346, <https://doi.org/10.1002/grl.50642>, 2013.
- 850 Hill, T., Chocholek, M., and Clement, R.: The case for increasing the statistical power of eddy covariance ecosystem studies: why, where and
851 how?, *Global Change Biology*, 23, 2154–2165, <https://doi.org/10.1111/gcb.13547>, 2017.
- 852 Hollinger, D. Y. and Richardson, A. D.: Uncertainty in eddy covariance measurements and its application to physiological models, *Tree*
853 *Physiology*, 25, 873–885, <https://doi.org/10.1093/treephys/25.7.873>, 2005.



- 854 Hollinger, D. Y., Aber, J., Dail, B., Davidson, E. A., Goltz, S. M., Hughes, H., Leclerc, M. Y., Lee, J. T., Richardson, A. D., Rodrigues, C.,
855 Scott, N., Achuatavari, D., and Walsh, J.: Spatial and temporal variability in forest–atmosphere CO₂ exchange, *Global Change Biology*,
856 10, 1689–1706, <https://doi.org/10.1111/j.1365-2486.2004.00847.x>, 2004.
- 857 Hollinger, S. E., Bernacchi, C. J., and Meyers, T. P.: Carbon budget of mature no-till ecosystem in North Central Region of the United States,
858 *Agricultural and Forest Meteorology*, 130, 59–69, <https://doi.org/10.1016/j.agrformet.2005.01.005>, 2005.
- 859 Hurlbert, S. H.: Pseudoreplication and the Design of Ecological Field Experiments, *Ecological Monographs*, 54, 187–211,
860 <https://doi.org/10.2307/1942661>, 1984.
- 861 Ibrom, A., Dellwik, E., Flyvbjerg, H., Jensen, N. O., and Pilegaard, K.: Strong low-pass filtering effects on water
862 vapour flux measurements with closed-path eddy correlation systems, *Agricultural and Forest Meteorology*, 147, 140–156,
863 <https://doi.org/10.1016/j.agrformet.2007.07.007>, 2007.
- 864 Jänicke, C., Goddard, A., Stein, S., Steinmann, H.-H., Lakes, T., Nendel, C., and Müller, D.: Field-level land-use data reveal
865 heterogeneous crop sequences with distinct regional differences in Germany, *European Journal of Agronomy*, 141, 126632,
866 <https://doi.org/10.1016/j.eja.2022.126632>, 2022.
- 867 Kaimal, J. C. and Finnigan, J. J.: *Atmospheric Boundary Layer Flows: Their Structure and Measurement*, Oxford University Press,
868 <https://doi.org/10.1093/oso/9780195062397.001.0001>, 1994.
- 869 Kanzler, M., Böhm, C., Mirck, J., Schmitt, D., and Veste, M.: Microclimate effects on evaporation and winter wheat (*Triticum aestivum* L.)
870 yield within a temperate agroforestry system, *Agroforestry Systems*, 93, 1821–1841, <https://doi.org/10.1007/s10457-018-0289-4>, 2019.
- 871 Kanzler, M., Böhm, C., and Freese, D.: The development of soil organic carbon under young black locust (*Robinia pseudoacacia* L.) trees at
872 a post-mining landscape in eastern Germany, *New Forests*, 52, 47–68, <https://doi.org/10.1007/s11056-020-09779-1>, 2021.
- 873 Katul, G., Hsieh, C.-I., Bowling, D., Clark, K., Shurpali, N., Turnipseed, A., Albertson, J., Tu, K., Hollinger, D., Evans, B., Offerle, B.,
874 Anderson, D., Ellsworth, D., Vogel, C., and Oren, R.: Spatial Variability of Turbulent Fluxes in the Roughness Sublayer of an Even-Aged
875 Pine Forest, *Boundary-Layer Meteorology*, 93, 1–28, <https://doi.org/10.1023/A:1002079602069>, 1999.
- 876 Kay, S., Rega, C., Moreno, G., Den Herder, M., Palma, J. H., Borek, R., Crous-Duran, J., Freese, D., Giannitsopoulos, M., Graves,
877 A., Jäger, M., Lamersdorf, N., Memedemin, D., Mosquera-Losada, R., Pantera, A., Paracchini, M. L., Paris, P., Roces-Díaz, J. V.,
878 Rolo, V., Rosati, A., Sandor, M., Smith, J., Szerencsits, E., Varga, A., Viaud, V., Wawer, R., Burgess, P. J., and Herzog, F.: Agro-
879 forestry creates carbon sinks whilst enhancing the environment in agricultural landscapes in Europe, *Land Use Policy*, 83, 581–593,
880 <https://doi.org/10.1016/j.landusepol.2019.02.025>, 2019.
- 881 Kljun, N., Rotach, M., and Schmid, H.: A Three-Dimensional Backward Lagrangian Footprint Model For A Wide Range Of Boundary-Layer
882 Stratifications, *Boundary-Layer Meteorology*, 103, 205–226, <https://doi.org/10.1023/A:1014556300021>, 2002.
- 883 Kljun, N., Calanca, P., Rotach, M. W., and Schmid, H. P.: A simple two-dimensional parameterisation for Flux Footprint Prediction (FFP),
884 *Geoscientific Model Development*, 8, 3695–3713, <https://doi.org/10.5194/gmd-8-3695-2015>, 2015.
- 885 Kutsch, W. L., Liu, C., Hörmann, G., and Herbst, M.: Spatial heterogeneity of ecosystem carbon fluxes in a broadleaved forest in Northern
886 Germany, *Global Change Biology*, 11, 70–88, <https://doi.org/10.1111/j.1365-2486.2004.00884.x>, 2005.
- 887 Launiainen, S., Vesala, T., Mölder, M., Mammarella, I., Smolander, S., Rannik, Ü., Kolari, P., Hari, P., Lindroth, A., and Katul, G. G.:
888 Vertical variability and effect of stability on turbulence characteristics down to the floor of a pine forest, *Tellus B: Chemical and Physical*
889 *Meteorology*, 59, 919, <https://doi.org/10.1111/j.1600-0889.2007.00313.x>, 2007.



- 890 Levy, P., Drewer, J., Jammet, M., Leeson, S., Friborg, T., Skiba, U., and Oijen, M. V.: Inference of spatial heterogeneity in surface
891 fluxes from eddy covariance data: A case study from a subarctic mire ecosystem, *Agricultural and Forest Meteorology*, 280, 107 783,
892 <https://doi.org/10.1016/j.agrformet.2019.107783>, 2020.
- 893 Lokupitiya, E., Denning, S., Paustian, K., Baker, I., Schaefer, K., Verma, S., Meyers, T., Bernacchi, C. J., Suyker, A., and Fischer, M.:
894 Incorporation of crop phenology in Simple Biosphere Model (SiBcrop) to improve land-atmosphere carbon exchanges from croplands,
895 *Biogeosciences*, 6, 969–986, <https://doi.org/10.5194/bg-6-969-2009>, 2009.
- 896 Lokupitiya, E., Denning, A. S., Schaefer, K., Ricciuto, D., Anderson, R., Arain, M. A., Baker, I., Barr, A. G., Chen, G., Chen, J. M., Ciais,
897 P., Cook, D. R., Dietze, M., El Maayar, M., Fischer, M., Grant, R., Hollinger, D., Izaurrealde, C., Jain, A., Kucharik, C., Li, Z., Liu, S., Li,
898 L., Matamala, R., Peylin, P., Price, D., Running, S. W., Sahoo, A., Sprintsin, M., Suyker, A. E., Tian, H., Tonitto, C., Torn, M., Verbeeck,
899 H., Verma, S. B., and Xue, Y.: Carbon and energy fluxes in cropland ecosystems: a model-data comparison, *Biogeochemistry*, 129, 53–76,
900 <https://doi.org/10.1007/s10533-016-0219-3>, 2016.
- 901 Lucas-Moffat, A. M., Schrader, F., Herbst, M., and Brümmer, C.: Multiple gap-filling for eddy covariance datasets, *Agricultural and Forest*
902 *Meteorology*, 325, 109 114, <https://doi.org/10.1016/j.agrformet.2022.109114>, 2022.
- 903 Mammarella, I. ., Kolari, P., Rinne, J. ., Keronen, P., Pumpanen, J. ., and Vesala, T.: Determining the contribution of vertical advection to the
904 net ecosystem exchange at Hyytiälä forest, Finland, *Tellus B: Chemical and Physical Meteorology*, 59, 900, [https://doi.org/10.1111/j.1600-](https://doi.org/10.1111/j.1600-0889.2007.00306.x)
905 [0889.2007.00306.x](https://doi.org/10.1111/j.1600-0889.2007.00306.x), 2007.
- 906 Mammarella, I., Launiainen, S., Gronholm, T., Keronen, P., Pumpanen, J., Rannik, Ü., and Vesala, T.: Relative Humidity Effect on the High-
907 Frequency Attenuation of Water Vapor Flux Measured by a Closed-Path Eddy Covariance System, *Journal of Atmospheric and Oceanic*
908 *Technology*, 26, 1856–1866, <https://doi.org/10.1175/2009JTECHA1179.1>, 2009.
- 909 Mammarella, I., Peltola, O., Nordbo, A., Järvi, L., and Rannik, Ü.: Quantifying the uncertainty of eddy covariance fluxes due to the use of
910 different software packages and combinations of processing steps in two contrasting ecosystems, *Atmospheric Measurement Techniques*,
911 9, 4915–4933, <https://doi.org/10.5194/amt-9-4915-2016>, 2016.
- 912 Markwitz, C.: Micrometeorological measurements and numerical simulations of turbulence and evapotranspiration over agroforestry, Doc-
913 toral Thesis, Georg-August-University Göttingen, <https://doi.org/10.53846/goediss-8477>, 2021.
- 914 Markwitz, C. and Siebicke, L.: Low-cost eddy covariance: a case study of evapotranspiration over agroforestry in Germany, *Atmospheric*
915 *Measurement Techniques*, 12, 4677–4696, <https://doi.org/10.5194/amt-12-4677-2019>, 2019.
- 916 Markwitz, C., Knohl, A., and Siebicke, L.: Evapotranspiration over agroforestry sites in Germany, *Biogeosciences*, 17, 5183–5208,
917 <https://doi.org/10.5194/bg-17-5183-2020>, 2020.
- 918 Mauder, M., Cuntz, M., Drüe, C., Graf, A., Rebmann, C., Schmid, H. P., Schmidt, M., and Steinbrecher, R.: A strategy for qual-
919 ity and uncertainty assessment of long-term eddy-covariance measurements, *Agricultural and Forest Meteorology*, 169, 122–135,
920 <https://doi.org/10.1016/j.agrformet.2012.09.006>, 2013.
- 921 Moncrieff, J., Malhi, Y., and Leuning, R.: The propagation of errors in long-term measurements of land-atmosphere fluxes of carbon and
922 water, *Global Change Biology*, 2, 231–240, <https://doi.org/10.1111/j.1365-2486.1996.tb00075.x>, 1996.
- 923 Muñoz-Sabater, J., Dutra, E., Agustí-Panareda, A., Albergel, C., Arduini, G., Balsamo, G., Boussetta, S., Choulga, M., Harrigan, S., Hers-
924 bach, H., Martens, B., Miralles, D. G., Piles, M., Rodríguez-Fernández, N. J., Zsoter, E., Buontempo, C., and Thépaut, J.-N.: ERA5-Land:
925 a state-of-the-art global reanalysis dataset for land applications, *Earth System Science Data*, 13, 4349–4383, [https://doi.org/10.5194/essd-](https://doi.org/10.5194/essd-13-4349-2021)
926 [13-4349-2021](https://doi.org/10.5194/essd-13-4349-2021), 2021.



- 927 Najibnia, S., Koocheki, A., Nassiri, M., and Porsa, H. M.: Water capture efficiency, use efficiency and productivity in
928 sole cropping and intercropping of rapeseed, bean and corn, *European Journal of Sustainable Development*, 3, 347–358,
929 <https://doi.org/10.14207/ejsd.2014.v3n4p347>, publisher: European Center of Sustainable Development, 2014.
- 930 Oren, R., Hsieh, C., Stoy, P., Albertson, J., McCarthy, H. R., Harrell, P., and Katul, G. G.: Estimating the uncertainty in annual net ecosystem
931 carbon exchange: spatial variation in turbulent fluxes and sampling errors in eddy-covariance measurements, *Global Change Biology*, 12,
932 883–896, <https://doi.org/10.1111/j.1365-2486.2006.01131.x>, 2006.
- 933 Papale, D., Reichstein, M., Aubinet, M., Canfora, E., Bernhofer, C., Kutsch, W., Longdoz, B., Rambal, S., Valentini, R., Vesala, T., and Yakir,
934 D.: Towards a standardized processing of Net Ecosystem Exchange measured with eddy covariance technique: algorithms and uncertainty
935 estimation, *Biogeosciences*, 3, 571–583, <https://doi.org/10.5194/bg-3-571-2006>, 2006.
- 936 Peltola, O., Hensen, A., Helfter, C., Beletti Marchesini, L., Bosveld, F. C., Van Den Bulk, W. C. M., Elbers, J. A., Haapanala, S., Holst, J.,
937 Laurila, T., Lindroth, A., Nemitz, E., Röckmann, T., Vermeulen, A. T., and Mammarella, I.: Evaluating the performance of commonly
938 used gas analysers for methane eddy covariance flux measurements: the InGOS inter-comparison field experiment, *Biogeosciences*, 11,
939 3163–3186, <https://doi.org/10.5194/bg-11-3163-2014>, 2014.
- 940 Peltola, O., Hensen, A., Beletti Marchesini, L., Helfter, C., Bosveld, F., Van Den Bulk, W., Haapanala, S., Van Huissteden,
941 J., Laurila, T., Lindroth, A., Nemitz, E., Röckmann, T., Vermeulen, A., and Mammarella, I.: Studying the spatial variability
942 of methane flux with five eddy covariance towers of varying height, *Agricultural and Forest Meteorology*, 214–215, 456–472,
943 <https://doi.org/10.1016/j.agrformet.2015.09.007>, 2015.
- 944 Pohanková, E., Hlavinka, P., Orság, M., Takáč, J., Kersebaum, K. C., Gobin, A., and Trnka, M.: Estimating the water use efficiency of spring
945 barley using crop models, *The Journal of Agricultural Science*, 156, 628–644, <https://doi.org/10.1017/S0021859618000060>, 2018.
- 946 Prabha, T. V., Leclerc, M. Y., and Baldocchi, D.: Comparison of In-Canopy Flux Footprints between Large-Eddy Simulation and the La-
947 grangian Simulation, *Journal of Applied Meteorology and Climatology*, 47, 2115–2128, <https://doi.org/10.1175/2008JAMC1814.1>, 2008.
- 948 Quandt, A., Neufeldt, H., and Gorman, K.: Climate change adaptation through agroforestry: opportunities and gaps, *Current Opinion in*
949 *Environmental Sustainability*, 60, 101 244, <https://doi.org/10.1016/j.cosust.2022.101244>, 2023.
- 950 Ran, Y., Li, X., Sun, R., Kljun, N., Zhang, L., Wang, X., and Zhu, G.: Spatial representativeness and uncertainty of eddy covariance carbon
951 flux measurements for upscaling net ecosystem productivity to the grid scale, *Agricultural and Forest Meteorology*, 230–231, 114–127,
952 <https://doi.org/10.1016/j.agrformet.2016.05.008>, 2016.
- 953 Rannik, Ü. and Vesala, T.: Autoregressive filtering versus linear detrending in estimation of fluxes by the eddy covariance method, *Boundary-*
954 *Layer Meteorology*, 91, 259–280, <https://doi.org/10.1023/A:1001840416858>, 1999.
- 955 Rannik, Ü., Kolari, P., Vesala, T., and Hari, P.: Uncertainties in measurement and modelling of net ecosystem exchange of a forest, *Agricul-*
956 *tural and Forest Meteorology*, 138, 244–257, <https://doi.org/10.1016/j.agrformet.2006.05.007>, 2006.
- 957 Rebmann, C., Kolle, O., Heinesch, B., Queck, R., Ibrom, A., and Aubinet, M.: Data acquisition and flux calculation, in: *Eddy Covariance: A*
958 *Practical Guide to Measurement and Data Analysis*, edited by Aubinet, M., Vesala, T., and Papale, D., Springer Netherlands, Dordrecht,
959 <https://doi.org/10.1007/978-94-007-2351-1>, 2012.
- 960 Reichstein, M., Falge, E., Baldocchi, D., Papale, D., Aubinet, M., Berbigier, P., Bernhofer, C., Buchmann, N., Gilmanov, T., Granier, A.,
961 Grünwald, T., Havránková, K., Ilvesniemi, H., Janous, D., Knohl, A., Laurila, T., Lohila, A., Loustau, D., Matteucci, G., Meyers, T.,
962 Miglietta, F., Ourcival, J., Pumpanen, J., Rambal, S., Rotenberg, E., Sanz, M., Tenhunen, J., Seufert, G., Vaccari, F., Vesala, T., Yakir,
963 D., and Valentini, R.: On the separation of net ecosystem exchange into assimilation and ecosystem respiration: review and improved
964 algorithm, *Global Change Biology*, 11, 1424–1439, <https://doi.org/10.1111/j.1365-2486.2005.001002.x>, 2005.



- Richardson, A. D., Hollinger, D. Y., Burba, G. G., Davis, K. J., Flanagan, L. B., Katul, G. G., William Munger, J., Ricciuto, D. M., Stoy, P. C., Suyker, A. E., Verma, S. B., and Wofsy, S. C.: A multi-site analysis of random error in tower-based measurements of carbon and energy fluxes, *Agricultural and Forest Meteorology*, 136, 1–18, <https://doi.org/10.1016/j.agrformet.2006.01.007>, 2006.
- Soegaard, H.: Carbon dioxide exchange over agricultural landscape using eddy correlation and footprint modelling, *Agricultural and Forest Meteorology*, 114, 153–173, [https://doi.org/10.1016/S0168-1923\(02\)00177-6](https://doi.org/10.1016/S0168-1923(02)00177-6), 2003.
- Stoy, P. C., Chu, H., Dahl, E., Cala, D. S., Shveytser, V., Wiesner, S., Desai, A. R., and Novick, K. A.: The global distribution of paired eddy covariance towers, <https://doi.org/10.1101/2023.03.03.530958>, 2023.
- Sun, F., Roderick, M. L., Farquhar, G. D., Lim, W. H., Zhang, Y., Bennett, N., and Roxburgh, S. H.: Partitioning the variance between space and time, *Geophysical Research Letters*, 37, 2010GL043 323, <https://doi.org/10.1029/2010GL043323>, 2010.
- Trouwloon, D., Streck, C., Chagas, T., and Martinus, G.: Understanding the Use of Carbon Credits by Companies: A Review of the Defining Elements of Corporate Climate Claims, *Global Challenges*, 7, 2200 158, <https://doi.org/10.1002/gch2.202200158>, 2023.
- van Ramshorst, J. G. V., Siebicke, L., Baumeister, M., Moyano, F. E., Knohl, A., and Markwitz, C.: Reducing Wind Erosion through Agroforestry: A Case Study Using Large Eddy Simulations, *Sustainability*, 14, 13 372, <https://doi.org/10.3390/su142013372>, 2022.
- van Ramshorst, J. G. V., Knohl, A., Callejas-Rodelas, J. Á., Clement, R., Hill, T. C., Siebicke, L., and Markwitz, C.: Lower-cost eddy covariance for CO₂ and H₂O fluxes over grassland and agroforestry, <https://doi.org/10.5194/amt-2024-30>, 2024.
- Vekuri, H., Tuovinen, J.-P., Kulmala, L., Papale, D., Kolari, P., Aurela, M., Laurila, T., Liski, J., and Lohila, A.: A widely-used eddy covariance gap-filling method creates systematic bias in carbon balance estimates, *Scientific Reports*, 13, 1720, <https://doi.org/10.1038/s41598-023-28827-2>, 2023.
- Veldkamp, E., Schmidt, M., Markwitz, C., Beule, L., Beuschel, R., Biertümpfel, A., Bischel, X., Duan, X., Gerjets, R., Göbel, L., Graß, R., Guerra, V., Heinlein, F., Komanda, M., Langhof, M., Luo, J., Potthoff, M., Van Ramshorst, J. G. V., Rudolf, C., Seserman, D.-M., Shao, G., Siebicke, L., Svoboda, N., Swieter, A., Carminati, A., Freese, D., Graf, T., Greef, J. M., Isselstein, J., Jansen, M., Karlovsky, P., Knohl, A., Lamersdorf, N., Priesack, E., Wachendorf, C., Wachendorf, M., and Corre, M. D.: Multifunctionality of temperate alley-cropping agroforestry outperforms open cropland and grassland, *Communications Earth & Environment*, 4, 20, <https://doi.org/10.1038/s43247-023-00680-1>, 2023.
- Vesala, T., Kljun, N., Rannik, Ü., Rinne, J., Sogachev, A., Markkanen, T., Sabelfeld, K., Foken, T., and Leclerc, M.: Flux and concentration footprint modelling: State of the art, *Environmental Pollution*, 152, 653–666, <https://doi.org/10.1016/j.envpol.2007.06.070>, 2008.
- Vuichard, N. and Papale, D.: Filling the gaps in meteorological continuous data measured at FLUXNET sites with ERA-Interim reanalysis, *Earth System Science Data*, 7, 157–171, <https://doi.org/10.5194/essd-7-157-2015>, 2015.
- Wang, H., Jia, G., Zhang, A., and Miao, C.: Assessment of Spatial Representativeness of Eddy Covariance Flux Data from Flux Tower to Regional Grid, *Remote Sensing*, 8, 742, <https://doi.org/10.3390/rs8090742>, 2016.
- Wilczak, J. M., Oncley, S. P., and Stage, S. A.: Sonic Anemometer Tilt Correction Algorithms, *Boundary-Layer Meteorology*, 99, 127–150, <https://doi.org/10.1023/A:1018966204465>, 2001.
- Winck, B. R., Bloor, J. M. G., and Klumpp, K.: Eighteen years of upland grassland carbon flux data: reference datasets, processing, and gap-filling procedure, *Scientific Data*, 10, 311, <https://doi.org/10.1038/s41597-023-02221-z>, 2023.
- Wohlfahrt, G., Hörtnagl, L., Hammerle, A., Graus, M., and Hansel, A.: Measuring eddy covariance fluxes of ozone with a slow-response analyser, *Atmospheric Environment*, 43, 4570–4576, <https://doi.org/10.1016/j.atmosenv.2009.06.031>, 2009.



- 1001 Wutzler, T., Lucas-Moffat, A., Migliavacca, M., Knauer, J., Sickel, K., Šigut, L., Menzer, O., and Reichstein, M.: Basic and extensible
1002 post-processing of eddy covariance flux data with REddyProc, Biogeosciences, 15, 5015–5030, <https://doi.org/10.5194/bg-15-5015-2018>,
1003 2018.
- 1004 Zhang, L., Guo, H., Jia, G., Wylie, B., Gilmanov, T., Howard, D., Ji, L., Xiao, J., Li, J., Yuan, W., Zhao, T., Chen, S., Zhou, G., and Kato,
1005 T.: Net ecosystem productivity of temperate grasslands in northern China: An upscaling study, Agricultural and Forest Meteorology, 184,
1006 71–81, <https://doi.org/10.1016/j.agrformet.2013.09.004>, 2014.